STEM CELLS

# Epigenetic regulation of p63 blocks squamous-to-neuroendocrine transdifferentiation in esophageal development and malignancy

**Yongchun Zhang[1,2,3]*†, Dimitris Karagiannis[4]†, Helu Liu[2,3,5]†, Mi Lin[2,3,6], Yinshan Fang[2,3], Ming Jiang[7], Xiao Chen[4]‡, Supriya Suresh[2,3], Haidi Huang[1], Junjun She[8,9], Feiyu Shi[8,9], Jiangying Liu[1], Dan Luo[1], J. Carlos Angel[4], Guangtan Lin[2,3,6], Patrick Yang[10], Wael El-Rifai[11,12], Alexander Zaika[11,12], Anthony E. Oro[13], Kuancan Liu[14], Anil K. Rustgi[3,15], Timothy C. Wang[3,15], Chao Lu[4,15]*, Jianwen Que[2,3,15]***



**While cell fate determination and maintenance are important in establishing and preserving tissue identity and function during development, aberrant cell fate transition leads to cancer cell heterogeneity and resistance to treatment. Here, we report an unexpected role for the transcription factor p63 (Trp63/TP63) in the fate choice of the squamous versus neuroendocrine lineage in esophageal development and malignancy. Deletion of *p63* results in extensive neuroendocrine differentiation in the developing mouse esophagus and esophageal progenitors derived from human embryonic stem cells. In human esophageal neuroendocrine carcinoma (eNEC) cells, p63 is transcriptionally silenced by EZH2-mediated H3K27 trimethylation (H3K27me3). Up-regulation of the major p63 isoform ΔNp63α, through either ectopic expression or EZH2 inhibition, promotes squamous transdifferentiation of eNEC cells. Together, these findings uncover p63 as a rheostat in coordinating the transition between squamous and neuroendocrine cell fates during esophageal development and tumor progression.**

## INTRODUCTION

Cell fate determination is critical for tissue development and homeostasis. Aberrant differentiation can lead to the ectopic emergence of cells that are incompatible with organ function. For example, the aberrant presence of acid-secreting cells in the esophagus contributes to pathological lesions known as inlet patches (*1*). In addition, abnormal cell-type conversions are found in premalignant lesions such as Barrett's metaplasia, where the stratified squamous epithelium is replaced by simple columnar cells in the distal portion of the esophagus (*2*–*4*). Chemotherapy and targeted therapy treatments have also been shown to induce a switch in tumor histology, such as androgen deprivation–induced prostate adenocarcinoma conversion into squamous cell carcinoma (SCC) (*5*, *6*). Moreover, neuroendocrine transdifferentiation was identified as a potential cause of drug resistance in several cancer types, including prostate adenocarcinoma and rectal adenocarcinoma (*7*, *8*). Chemoradiotherapy can also cause esophageal cancer to switch from SCC to neuroendocrine carcinoma (*9*). Despite an increasing appreciation of the prevalence and significance of such tumor lineage plasticity, the underlying molecular mechanisms remain largely unknown.

The adult esophagus is lined with a stratified squamous epithelium, which starts as simple columnar cells in the early foregut (*10*, *11*). Genetic studies have shown that the bone morphogenetic protein (BMP) pathway plays a critical role in this transformation, involving the specification of basal progenitor cells into squamous epithelium (*12*). Downstream of BMP signaling, p63 (Trp63 in mice, TP63 in humans) is a key master transcription factor specifically enriched in basal progenitor cells (*13*). Deletion of *p63* blocks the formation of stratified squamous epithelium in the esophagus and skin (*14*–*17*). In skin keratinocytes, p63 has been shown to modulate the epigenomic landscape through the recruitment of various chromatin regulators (*18*–*20*). Similarly, the depletion of p63 in the prostate epithelium results in the loss of basal cells while acquiring a goblet cell–like phenotype (*21*, *22*). Ciliated cells and mucus-producing cells have been reported to be increased in the esophagus of *p63*-null mutants (*13*, *23*). However, how p63 is involved in cell fate determination in esophageal progenitor cells remains incompletely understood.

Neuroendocrine cells play important roles in chemoreception, mechanotransduction, and immune cell responses in the stomach, intestine, and lung (*24*–*26*). Although Merkel cells, one type of neuroendocrine cell, have been detected in the human esophagus (*27*),

[1]State Key Laboratory of Microbial Metabolism and Joint International Research Laboratory of Metabolic and Developmental Sciences, School of Life Sciences and Biotechnology, Shanghai Jiao Tong University, Shanghai 200240, China. [2]Columbia Center for Human Development, Department of Medicine, Vagelos College of Physicians and Surgeons, Columbia University Irving Medical Center, New York, NY 10032, USA. [3]Division of Digestive and Liver Diseases, Department of Medicine, Vagelos College of Physicians and Surgeons, Columbia University Irving Medical Center, New York, NY 10032, USA. [4]Department of Genetics and Development, Columbia University Irving Medical Center, New York, NY 10032, USA. [5]Institute of Deep-sea Science and Engineering, Chinese Academy of Sciences, Sanya 572000, Hainan, China. [6]Department of Gastric Surgery, Fujian Medical University Union Hospital, Fuzhou 350001, Fujian, China. [7]Center for Genetic Medicine, The Fourth Affiliated Hospital, Zhejiang University School of Medicine, Hangzhou 310030, Zhejiang, China. [8]Department of General Surgery, The First Affiliated Hospital of Xi'an Jiaotong University, Xi'an 710061, Shaanxi, China. [9]Center for Gut Microbiome Research, Med-X Institute, The First Affiliated Hospital of Xi'an Jiaotong University, Xi'an 710061, Shaanxi, China. [10]Department of Internal Medicine, Westchester Medical Center/New York Medical College, Valhalla, NY 10595, USA. [11]Department of Surgery and Sylvester Comprehensive Cancer Center, University of Miami, Miami, FL 33136, USA. [12]Miami Veterans Affairs Healthcare System, Miami, FL 33136, USA. [13]Programin Epithelial Biology, Stanford University School of Medicine, Stanford 94305, CA, USA. [14]Central Laboratory, Xiang'an Hospital, School of Medicine, Xiamen University, Xiamen 361102, Fujian, China. [15]Herbert Irving Comprehensive Cancer Center, Vagelos College of Physicians and Surgeons, Columbia University Irving Medical Center, New York, NY 10032, USA.
*Corresponding author. Email: yongchun_zhang@sjtu.edu.cn (Y.Z.); cl3684@cumc.columbia.edu (C.L.); jq2240@cumc.columbia.edu (J.Q.)
†These authors contributed equally to this work.
‡Present address: Marine College, Shandong University, Weihai 264209, China.

their function remains unknown. In the mouse esophagus, the existence of neuroendocrine cells has not been reported. Notably, neuroendocrine carcinoma also occurs in the esophagus, accounting for 0.4 to 2.8% of human esophageal cancers (*28*). Esophageal neuroendocrine carcinoma (eNEC) is highly aggressive and composed of cancer cells characterized by high expression levels of neuroendocrine cell markers such as synaptophysin (SYP) and chromogranin (CHGA), similar to small cell lung cancer (SCLC) (*29*, *30*). Note that eNECs are negative for the expression of p63 (*31*), yet genome sequencing reveals no mutation in the gene encoding p63 (*32*), suggesting an epigenetic mechanism underlying p63 silencing during tumor progression.

Histone posttranslational modifications, such as methylation and acetylation, modulate the structure of chromatin and affect gene transcription. The trimethylation of lysine-27 on histone H3 (H3K27me3) is catalyzed by the methyltransferase enhancer of zeste homolog 2 (EZH2), a core subunit of polycomb repressive complex 2 (*33*). H3K27me3 generally represses the transcription of genes that are essential for lineage specification (*34*). Hence, EZH2 is important for tissue development, homeostasis, and tumorigenesis (*33*). By contrast, histone acetylation generally activates gene transcription (*35*). Histone acetylation is regulated by both histone acetyltransferase (e.g., p300/CBP) and histone deacetylases (HDACs) (*36*). In addition, the bromodomain and extraterminal (BET) protein family, including BRD2, BRD3, BRD4, and BRDT, recognizes and binds to acetylated histone lysine residues to recruit RNA polymerase II to promote gene transcription (*37*). Accordingly, histone acetylation markers such as H3K27 acetylation (H3K27ac) demarcate active cis-regulatory elements critical for tissue development (*38*).

Here, we report that epigenetic regulation of p63 is critical for esophageal development and tumor lineage plasticity. p63 acts as a conserved guardian against neuroendocrine cell fate, and *p63* deletion leads to abundant neuroendocrine cell differentiation in the developing esophagus. Conversely, p63 overexpression confers squamous cell differentiation in eNEC cells. We further show that p63 expression is epigenetically silenced by H3K27me3 in eNEC cells. Treatment with EZH2 inhibitors reduces H3K27me3, leading to the expression of p63 and squamous identity genes in eNEC organoids.

## RESULTS

### p63 represses neuroendocrine cell differentiation in the developing mouse esophagus

We and others have shown that deletion of *p63* causes the emergence of mucociliated cells in the esophagus (*3*, *13*, *23*). To comprehensively identify the cell types present in the *p63*-null developing esophagus, we compared gene expression of the esophageal epithelium between *p63 knockout* (*KO*) mutants and the littermate *wild-type* (*WT*) controls at E12.5 (Fig. 1A). Differential expression analysis revealed that 954 and 703 genes were significantly up-regulated and down-regulated in *p63 KO* mutants, respectively (Fig. 1B and table S1). Gene ontology analysis and gene set enrichment analysis (GSEA) revealed a notable impact of p63 loss on cell fate pathways and related biological processes (Fig. 1, C to E, and fig. S1). Specifically, we observed down-regulation of genes associated with basal and squamous cell identity and extracellular matrix organization (Fig. 1, C and D, and fig. S1). The basal cell signature genes *Krt5* and *Krt15* and adhesion molecules including *Itga3*, *Itga6*, *Itgb4*, and *Lamb3* were reduced in the mutant esophageal epithelium (Fig. 1F). As expected, the expression levels of the ciliated genes *Tuba1a* and *Tubb4a* and the columnar cell keratins *Krt7*, *Krt8*, and *Krt18* were significantly increased upon *p63* deletion (Fig. 1F). We found that genes up-regulated in mutants were enriched for those regulating neuroendocrine cell identity and neurotransmitter processes (Fig. 1, C and E). We observed up-regulation of neuroendocrine cell signature genes including *Ascl1*, *Insm1*, *Cgrp*, *Syp*, *Chga*, *Chgb*, *Edn1*, *Eno2*, *Cck*, *Uch1*, *Gfi1*, and *Ncam1* in mutants (Fig. 1F). We further used immunofluorescence (IF) staining to confirm the ectopic presence of insulinoma-associated protein 1 (INSM1)-expressing neuroendocrine progenitor cells in the mutant but not WT esophagus (Fig. 1G). We also observed abundant mature neuroendocrine cells expressing CGRP and SYP in the mutant esophagus at embryonic day 18.5 (E18.5; Fig. 1, H and I). These data confirm that *p63* deletion leads to the ectopic presence of neuroendocrine cells, suggesting that p63 is required for protecting against aberrant neuroendocrine differentiation during esophageal development.

To determine whether neuroendocrine cells originated from p63-expressing esophageal progenitor cells, we conducted lineage tracing experiments. Tamoxifen was administered to $p63^{CreERT2/+};R26^{tdTomato}$ (*control*) and $p63^{CreERT2/CreERT2};R26^{tdTomato}$ (*p63 KO*) mouse embryos at E10.5, and tissues were harvested at E18.5. We observed tdTomato expression in the esophagus and forestomach in both *control* and *p63 KO* mutants (Fig. 2A). Immunostaining further revealed tdTomato expression in all esophageal epithelial cells of both *control* and *p63 KO* mutants, with a subset of *p63 KO* esophageal epithelial cells being neuroendocrine cells, as evidenced by co-expression of SYP and tdTomato (Fig. 2B). These results indicated that the ectopic neuroendocrine cells were derived from the *p63 KO* esophageal epithelium. Next, we conducted single-cell RNA sequencing on E18.5 esophageal epithelial cells. Uniform manifold approximation and projection (UMAP) analysis revealed five cell types, including proliferating basal cells, non-proliferating basal cells, suprabasal cells, neuroendocrine cells, and ciliated cells (Fig. 2, C to M). Notably, neuroendocrine cells represented 24.08% of the cells identified in the *p63 KO* mutants (Fig. 2F). In contrast, despite a few cells (0.05%) being assigned as neuroendocrine cells in *WT* mice (Fig. 2F), no such cells can be detected by immunostaining (Fig. 1, G to I). Moreover, pseudo-time trajectory analysis showed that basal cells served as the origin of all other epithelial cell types. Intriguingly, neuroendocrine epithelial cells followed a distinct differentiation path from suprabasal cells, indicating activation of a neuroendocrine cell transcriptional program upon *p63* deletion (Fig. 2N).

### p63 plays a conserved role in repressing neuroendocrine cell fate in hESC-derived esophageal progenitor cells

To address whether p63 plays a similar role in inhibiting neuroendocrine cell fate in human esophageal progenitor cells (hEPCs), we deleted *p63* in the H9 human embryonic stem cell (hESC) line. We then differentiated H9 into EPCs in a two-dimensional (2D) system using the protocol that we previously described (*39*, *40*). We detected increased expression of the neuroendocrine genes *ASCL1*, *INSM1*, *SYP*, *CGRP*, *CHGA*, and *SST* at day 24 of differentiation (Fig. 3A), and $ASCL1^{+}$ neuroendocrine cells were present among EPCs following *p63* deletion (Fig. 3B). In addition, we embedded endodermal spheroids in Matrigel and induced them to form 3D esophageal organoids (Fig. 3C). We collected the organoids after 7 weeks in culture and determined the expression of genes marking basal cells versus neuroendocrine cells. Immunostaining for the

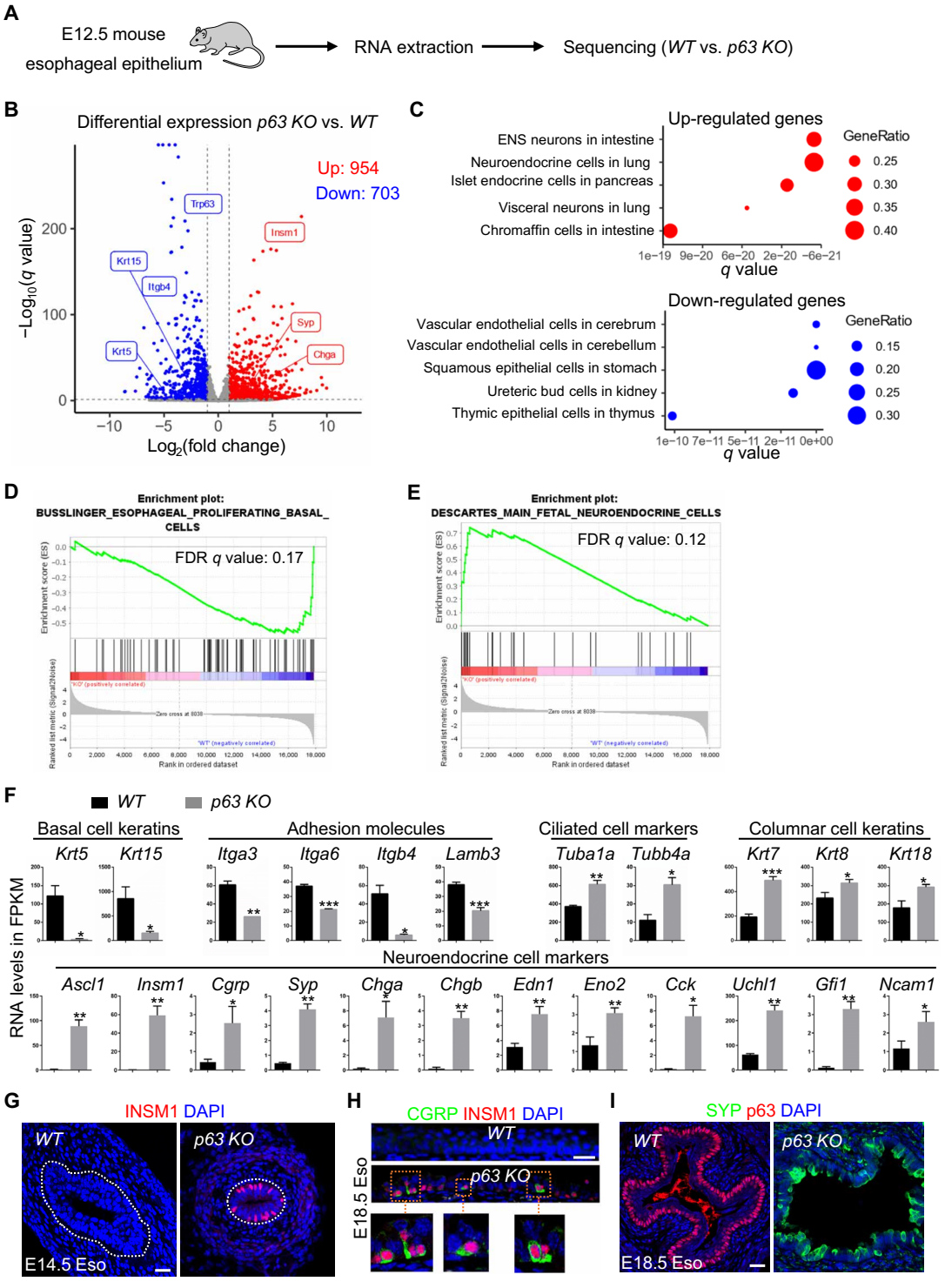


**Fig. 1. Loss of p63 leads to neuroendocrine cell differentiation in the developing mouse esophagus.** (**A**) Schematics showing the epithelial isolation, RNA extraction, and sequencing of the esophagus from *WT* and *p63 KO* mice. $n = 3$ per genotype. (**B**) Volcano plot of differentially expressed genes between *WT* and *p63 KO* mouse esophageal epithelium. Noted are genes involved in squamous and neuroendocrine cell identity. (**C**) Cell types and tissues gene ontology of genes up-regulated (red) and down-regulated (blue) in *p63 KO* mouse esophageal epithelium annotated by Descartes Cell Types and Tissues 2021. (**D** and **E**) Gene set enrichment analysis (GSEA) indicating down-regulation of the esophageal basal cell signature genes and up-regulation of the neuroendocrine cell signature genes. FDR, false discovery rate. (**F**) *p63* deletion reduces the transcript levels of the basal cell keratins *Krt5* and *Krt15* and the adhesion molecules *Itga3*, *Itga6*, *Itgb4*, and *Lamb3* but increases the levels of the ciliated cell genes *Tuba1a* and *Tubb4a* and neuroendocrine cell signature genes including *Ascl1*, *Insm1*, *Cgrp*, *Syp*, *Chga*, *Chgb*, *Edn1*, *Eno2*, *Cck*, *Uch1*, *Gfi1*, and *Ncam1*. $^*P < 0.05$, $^{**}P < 0.01$, and $^{***}P < 0.001$. FPKM, fragments per kilobase of transcript per million mapped reads. (**G**) The neuroendocrine cell marker INSM1 is ectopically expressed in the epithelium of E14.5 *p63 KO* esophagus. (**H** and **I**) The neuroendocrine markers INSM1, CGRP, and SYP are expressed in the epithelium of *p63 KO* esophagus. Eso, esophagus. Scale bars, 20 μm. DAPI, 4′,6-diamidino-2-phenylindole.

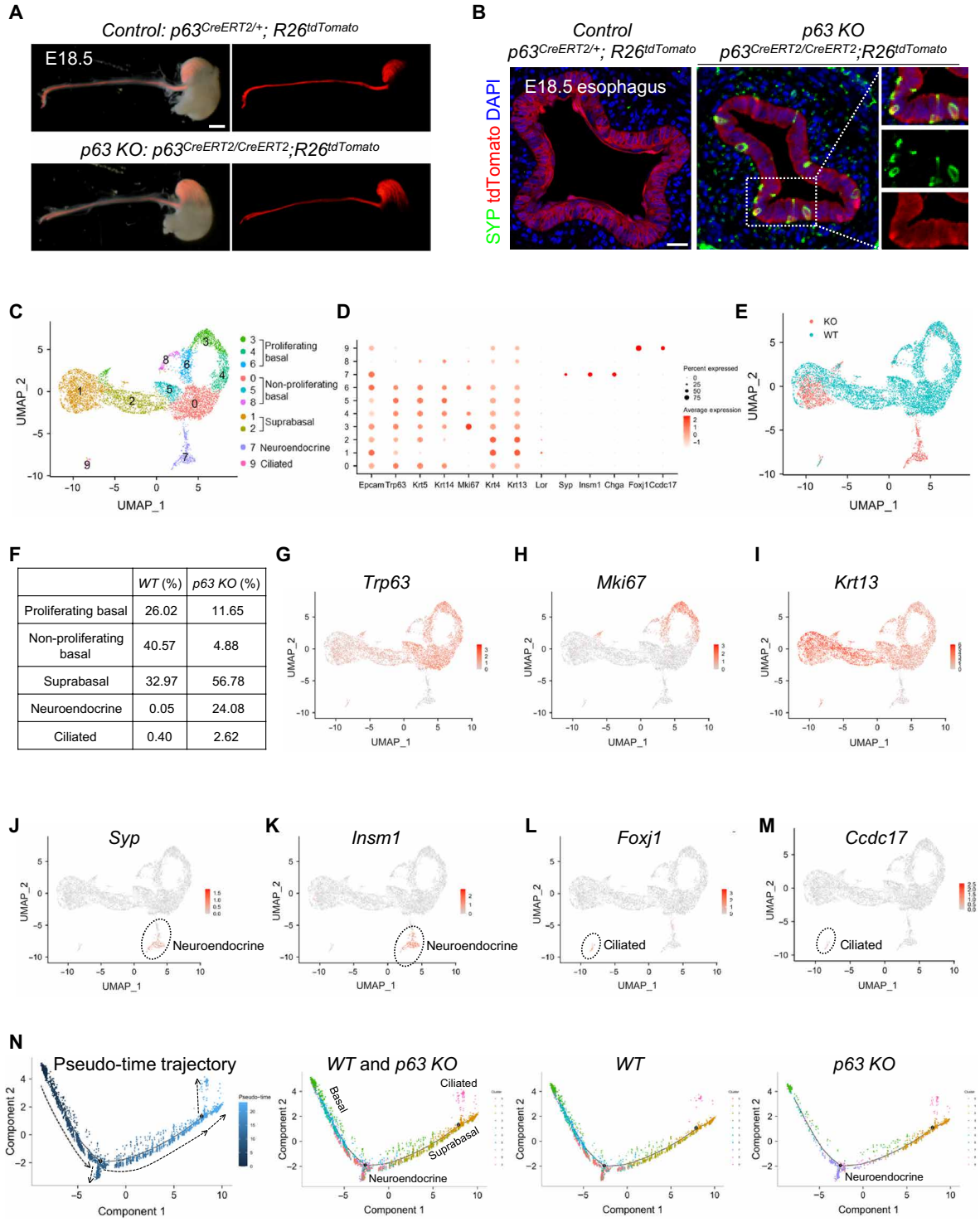


**Fig. 2. Lineage tracing and high-dimensional single-cell trajectory analysis reveal p63-expressing progenitor cells as the cellular source of neuroendocrine cells within the esophageal epithelium.** (**A**) *p63*$^{CreERT2/+}$;*R26*$^{tdTomato}$ (*control*) and *p63*$^{CreERT2/CreERT2}$;*R26*$^{tdTomato}$ (*p63 KO*) mouse embryos administered with tamoxifen by oral gavage at E10.5 and tissues were harvested at E18.5. Scale bar, 1 mm. (**B**) Immunostaining of SYP and tdTomato. Note that the whole esophageal epithelium expresses tdTomato in both *WT* and *p63 KO* mice and the ectopic presence of SYP$^{+}$ neuroendocrine cells in *p63 KO* mutants. Scale bar, 20 μm. (**C**) UMAP plot of single-cell RNA sequencing data of E18.5 *p63 KO* and *WT* esophageal epithelial cells. (**D**) Dot plot depicting expression of epithelial cell marker Epcam; basal cell markers *Trp63*, *Krt5*, and *Krt14*; proliferation marker *Mki67*; suprabasal cell differentiation markers *Krt4* and *Krt13*; neuroendocrine cell markers *Syp*, *Insm1*, and *Chga*; and ciliated cell markers *Foxj1* and *Ccdc17*. (**E** and **F**) Percentage of each type of cell in the *p63 KO* and *WT* embryos. Notably, 0.05% of cells were assigned as neuroendocrine cells, but no such cells can be detected with immunostaining in *WT* mice. (**G** to **M**) Feature plot depicting individual gene expression. (**N**) Pseudo-time trajectory analysis of different cell types.

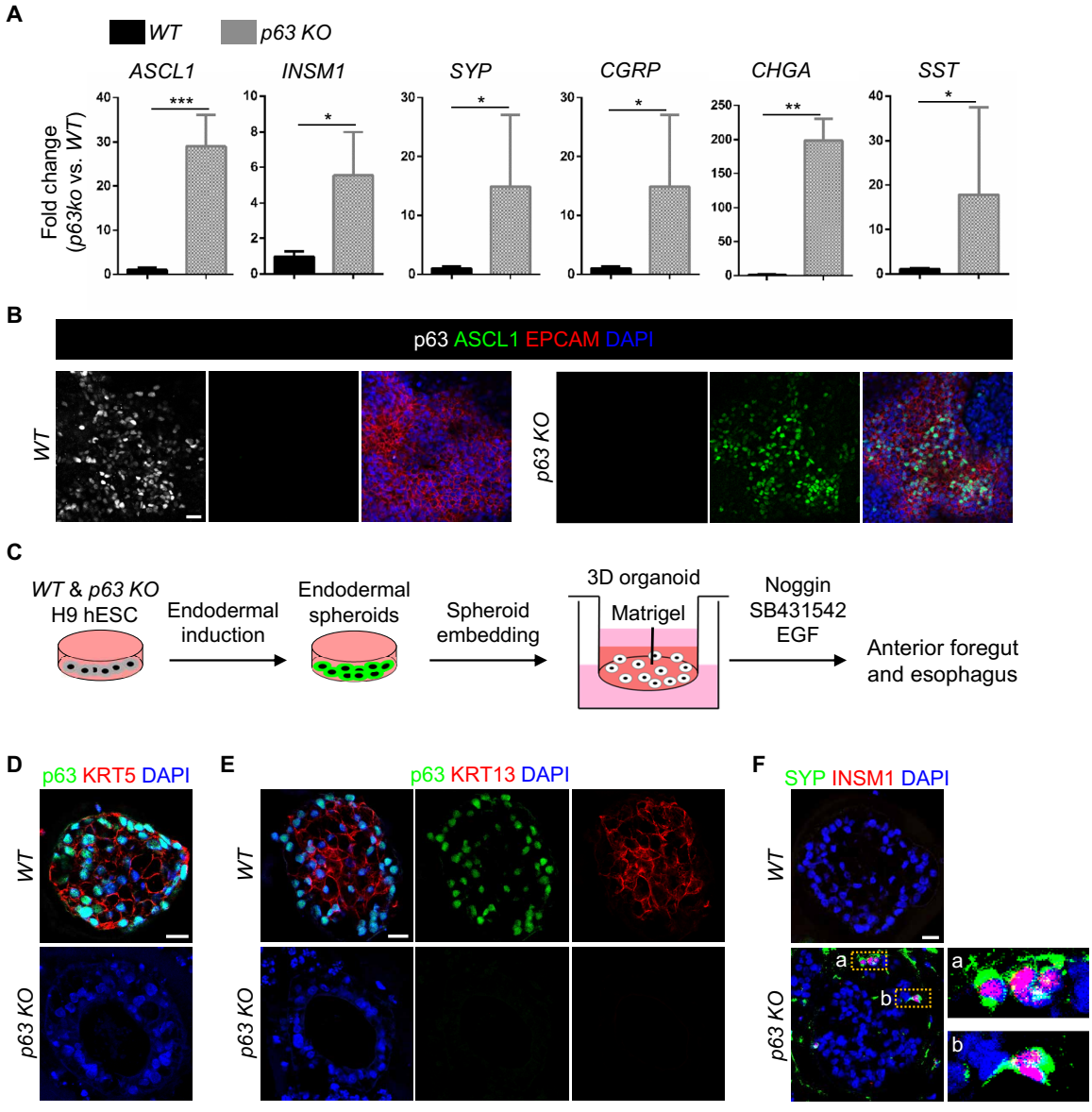


**Fig. 3. p63 deletion leads to neuroendocrine differentiation of esophageal progenitor cells derived from hESCs.** (**A** and **B**) *p63* deletion leads to ectopic neuroendocrine cell differentiation, shown by the increased transcript levels of *ASCL1*, *INSM1*, *SYP*, *CGRP*, *CHGA*, and *SST* (A) and ectopic expression of ASCL1 protein (B). Black bar, *WT*; gray bar, *p63 KO*. **P* < 0.05, ***P* < 0.01, and ****P* < 0.001. (**C**) Schematics showing the differentiation of H9 hESCs into esophageal progenitor cells and the formation of esophageal organoids. Endodermal organoids derived from H9 hESCs cells were embedded in Matrigel and cultured in the presence of Noggin, SB431542, and EGF for 7 weeks to form esophageal organoids. (**D**) *p63* deletion leads to the loss of KRT5 expression in hESC-derived esophageal cells. (**E**) *p63* deletion perturbs the formation of stratified esophageal organoids. Note that the *WT* organoids express high levels of p63 and KRT13 in the periphery and center, respectively. The pattern is lost in *p63 KO* organoids. (**F**) p63 deletion leads to the ectopic expression of INSM1 and SYP (yellow boxes) in hESC-derived esophageal organoids. Scale bars, 20 μm.

basal cell markers p63 and KRT5 and the suprabasal cell marker KRT13 revealed a loss of squamous stratification in the *p63 KO* mutants compared to the *WT* esophageal organoids (Fig. 3, D to E). We observed the ectopic presence of $INSM1^{+}SYP^{+}$ neuroendocrine cells in organoids formed by *p63*-null hESC-derived EPCs (Fig. 3F). By contrast, $INSM1^{+}SYP^{+}$ cells were not detected in the organoids formed by control hESC-derived EPCs (Fig. 3F). Together, these findings suggest a conserved role for p63 in repressing neuroendocrine cell differentiation during the development of the human esophagus.

## p63 expression is repressed by EZH2-mediated H3K27 methylation in eNECs

Because *p63* deletion led to the ectopic presence of neuroendocrine cells in the esophagus, we hypothesized that p63 inactivation is required to maintain esophageal neuroendocrine cell identity. While neuroendocrine cells have yet to be identified in the mouse esophagus, Merkel cells have been detected in the human esophagus. Notably, p63 expression is lost in human eNEC (*29*, *31*). We confirmed that p63 was not detected in $INSM1^{+}$ neuroendocrine cancer cells in human eNEC specimens, whereas neighboring

basal cells expressed high levels of p63 (Fig. 4A). Mutational profiling indicated that *p63* is not genetically mutated in a large cohort of eNECs (*32*). We therefore asked whether p63 is silenced through epigenetic mechanisms.

The *TP63* gene encoding human p63 harbors two alternative promoters, resulting in TAp63 isoforms with the N-terminal transactivation (TA) domain or ΔNp63 isoforms lacking the TA domain (*41*). We first tested whether TAp63 and ΔNp63 expression is modulated epigenetically by screening a panel of chromatin regulator inhibitors in a human eNEC cell line (TYUC-1) (Fig. 4B and fig. S2A). We found that inhibition of EZH2, the histone methyltransferase that catalyzes H3K27me3 deposition, with the Food and Drug Administration (FDA)–approved small-molecule inhibitor EPZ-6438 induced the highest expression levels of ΔNp63 (Fig. 4C), indicating that H3K27me3 represses ΔNp63 expression in eNECs. In addition, inhibition of HDACs with either Vorinostat or Romidepsin increased ΔNp63 expression (Fig. 4C). EZH2 and HDAC inhibitors also modestly up-regulated the expression of TAp63 (Fig. 4C). Conversely, inhibition of histone acetyltransferase p300/CBP and BET proteins, "readers" of histone lysine acetylation, reduced TAp63 and ΔNp63 expression (Fig. 4C). These results suggest that the post-translational modification state of histone H3K27 (acetylation versus methylation) has a direct effect on p63 expression. Consistently, the transcriptional activating effect of EZH2 inhibition (EZH2i; EPZ-6438) on ΔNp63 was abolished by co-treatments with either BET protein (JQ1) or CBP/p300 (A485) inhibitors (Fig. 4D), suggesting that histone acetylation and BET protein binding are required for ΔNp63 expression following H3K27me3 depletion. We also found that EPZ-6438 treatment increased the protein abundance of p63 in TYUC-1 cells (Fig. 4, E and F).

To assess the chromatin landscape following EZH2i, we performed cleavage under targets and tagmentation (CUT&Tag) of H3K27me3, H3K27ac, and BRD4 upon EPZ-6438 treatment (Fig. 4G). As expected, H3K27me3 was enriched in the *TP63* locus, as assessed by both CUT&Tag and chromatin immunoprecipitation sequencing (ChIP-seq; fig. S2B), and was lost upon EPZ-6438 treatment in TYUC-1 cells (Fig. 4G). Moreover, EPZ-6438–treated cells gained two peaks of H3K27ac and BRD4 binding at putative intronic enhancers close to the transcription start site (TSS) of ΔNp63 isoforms (Fig. 4G, right). Notably, reanalysis of ChIP-seq data of esophageal epithelium from ENCODE found the presence of H3K27ac peaks at these sites, indicating that they represent physiologically relevant squamous-specific cis-regulatory elements associated with p63 expression (Fig. 4G). Together, these results suggest that epigenetic modifications mediated by EZH2 play a critical role in silencing p63 in eNECs.

### ΔNp63α isoform promotes the squamous transdifferentiation program in eNEC cells

To investigate whether restoration of p63 expression affects neuroendocrine cell identity, we first used a doxycycline-inducible system to overexpress p63 in TYUC-1 cells (Fig. 5A). We chose to express two major p63 isoforms, TAp63α and ΔNp63α (*41*), both present in the esophagus, to determine their effects on altering the cell fate of eNEC. RNA sequencing indicated that ectopic Δ*Np63*α expression induced higher transcription of genes associated with squamous identity than *TAp63*α (Fig. 5B). In agreement with this, the majority of ΔNp63α-expressing cells also expressed KRT5, in contrast to TAp63α$^+$ cells (Fig. 5, C and D).

To exclude the possibility that the differential induction of squamous identity genes is due to the differences in p63 isoform expression levels, we measured the percentage of p63$^+$ cells as well as p63 IF signal intensity in TYUC-1 organoids and found no significant differences (fig. S3, A and B). In addition, we measured *KRT5* expression using quantitative real-time polymerase chain reaction (qRT-PCR) at a concentration of doxycycline where *TAp63*α and Δ*Np63*α were induced at comparable levels. We confirmed that ΔNp63α was more potent in activating KRT5 expression (fig. S3C). These results are consistent with the relatively dominant role of ΔNp63 over TAp63 in the regulation of keratin gene expression during keratinocyte differentiation (*42*).

To determine whether ectopically expressed ΔNp63α directly activates squamous genes in eNEC cells, we assessed ΔNp63α genome-wide binding using CUT&Tag in TYUC-1 cells where ΔNp63α expression was induced for 16 hours. Motif analysis of ΔNp63α peaks confirmed the enrichment of p63 binding motif as expected (fig. S3D). Peak annotation indicated that the majority of ΔNp63α peaks were found within gene promoters and introns (fig. S3E), consistent with the notion that p63 regulates gene expression through binding to cis-regulatory elements (*43*). ΔNp63α peaks were identified close to the promoters of the squamous identity genes, including *KRT5*, *KRT15*, *LAMB3*, and *ITGB4*, suggesting a direct regulation of their expression (Fig. 5, E to H).

We further characterized the transcriptomic changes in TYUC-1 cells following ΔNp63α overexpression for 6 days (Fig. 6A). Differential gene expression analysis indicated that more genes were up-regulated than down-regulated (207 versus 41), suggesting a positive role for ΔNp63α in gene expression (Fig. 6A and table S2). Moreover, we observed an enrichment of squamous genes in the up-regulated gene list (Fig. 6B and fig. S4A), as well as an increasing predominance of squamous signature gene expression over time (Fig. 6C). Notably, among 5877 genes that were associated with at least one ΔNp63α peak, less than 2% (90) were up-regulated upon ΔNp63α overexpression (Fig. 6D), suggesting that ΔNp63α binding alone is often not sufficient to increase the expression of its target genes.

We investigated why a small subset of all ΔNp63α-bound genes were up-regulated by ΔNp63α overexpression. We found that up-regulated genes had on average lower baseline expression levels compared to genes that were down-regulated or not differentially expressed after ΔNp63α overexpression (fig. S4B). Furthermore, up-regulated genes were associated with ΔNp63α peaks that localized closer to the TSS (fig. S4C) and had higher CUT&Tag signals (fig. S4D). Last, we performed motif enrichment analyses and found that, compared to ΔNp63α peaks associated with non–up-regulated genes, peaks associated with up-regulated genes had fewer significantly enriched ($q < 0.05$) transcription factor (TF) motifs beyond p63 (12 versus > 127; tables S3 and S4). This suggests that ΔNp63α–up-regulated genes are less likely to require additional cofactors for activation. These results are in agreement with previous work showing that additional chromatin features, such as the presence of histone H3 acetylation, are required for efficient induction of gene expression by p63 (*43*).

We further determined the effect of ΔNp63α on the squamous transdifferentiation in TYUC-1 tumor organoids. ΔNp63α overexpression resulted in the ectopic protein expression of basal cell markers KRT5, KRT14, and KRT15 (Figs. 5C and 6, E and F, and fig. S4E), as well as differentiated squamous cell markers KRT4 and

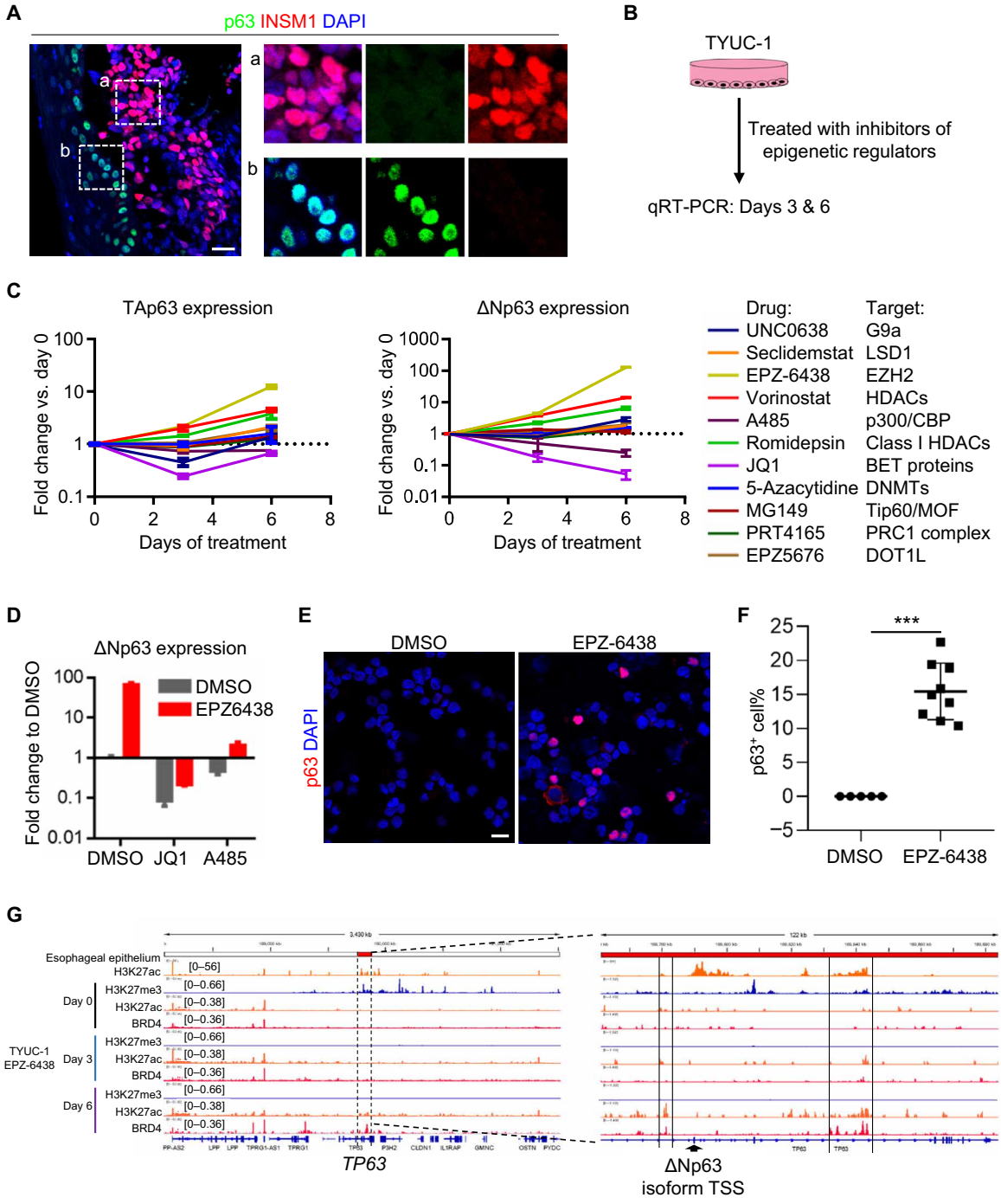


**Fig. 4. ΔNp63 expression is regulated by methylation and acetylation of histone H3 lysine-27.** (**A**) p63 and INSM1 staining in human eNEC specimens. Scale bar, 20 μm. (**B**) Schematics showing that TYUC-1 eNEC cells were treated with inhibitors of epigenetic regulators, and gene expression was analyzed by quantitative real-time polymerase chain reaction (qRT-PCR). (**C**) The transcript levels of *TAp63* and Δ*Np63* in TYUC-1 eNEC cells treated with various epigenetic inhibitors. Note that the EZH2 inhibitor EPZ-6438 increased the expression of *TAp63* and Δ*Np63* to the highest levels compared to other inhibitors. (**D**) Transcript levels of Δ*Np63* in TYUC-1 cells treated with EPZ-6438 alone or in combination with JQ1 or A485. (**E** and **F**) IF staining and quantification of $p63^+$ cells in EPZ-6438–treated TYUC-1 cells. Note that p63 is expressed in the EPZ-6438–treated group but not in the dimethyl sulfoxide (DMSO)–treated group. ***$P < 0.001$. Scale bar, 20 μm. (**G**) Genome browser view at the *TP63* locus showing esophagus epithelium H3K27ac ChIP-seq (ENCODE SRX3205374) and TYUC-1 cell H3K27me3, H3K27ac, and BRD4 cleavage under targets and tagmentation (CUT&Tag) upon treatment with EPZ-6438 for 3 and 6 days. Indicated are putative enhancer elements near the ΔNp63 isoform transcription start site (TSS) where H3K27 methylation is lost, and acetylation is restored.

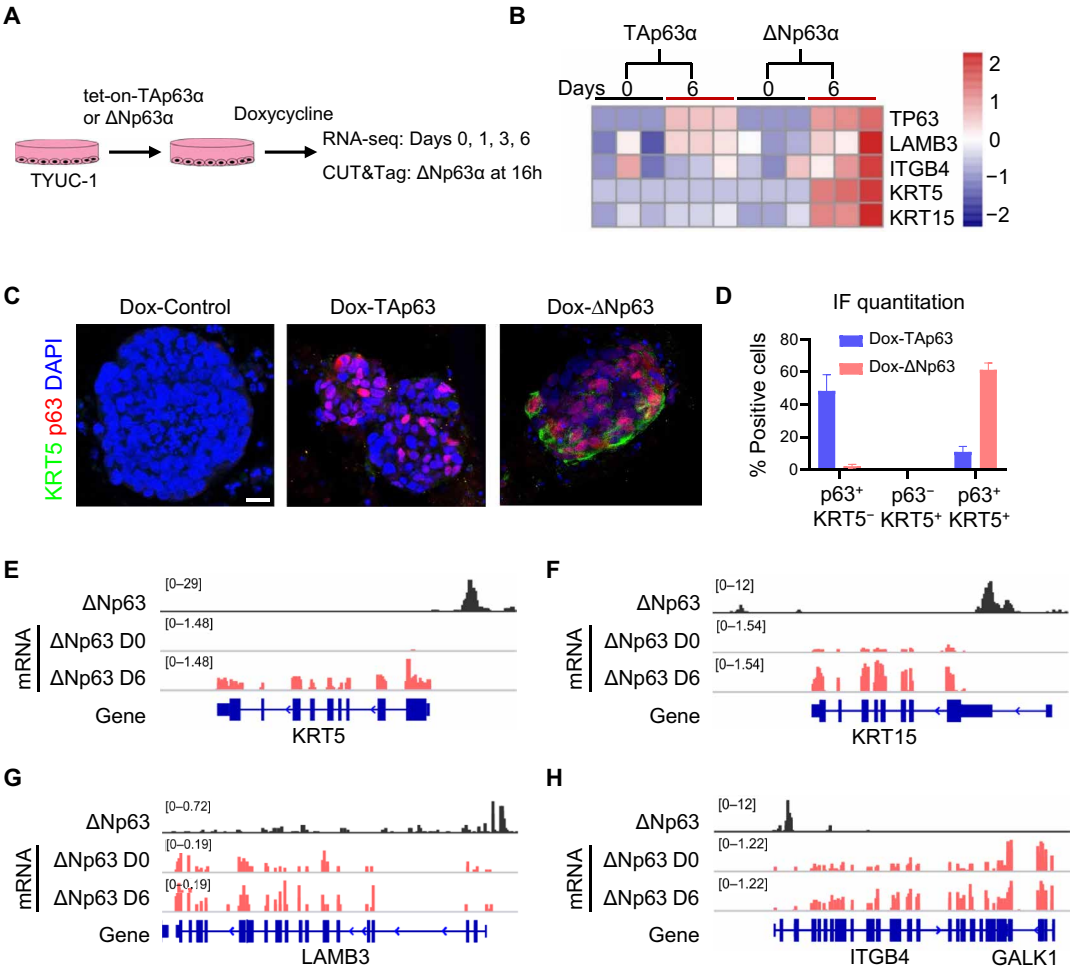


**Fig. 5. When overexpressed ΔNp63 isoform binds to and promotes the expression of squamous identity genes in esophageal neuroendocrine cancer cells.** (**A**) Schematics showing overexpressing ΔNp63α and TAp63α in TYUC-1 cells. Gene expression was analyzed by RNA sequencing (RNA-seq; $n = 3$), and ΔNp63α binding sites on chromatin were profiled by CUT&Tag assays ($n = 2$). (**B**) A heatmap of the transcript levels of squamous cell markers. Note that *KRT5* and *KRT15* genes were only induced by ΔNp63α. (**C**) IF staining of p63 and KRT5 in TYUC-1 tumor organoids with doxycycline-induced overexpression of TAp63α and ΔNp63α versus the untreated (control). Scale bar, 20 μm. (**D**) Quantitation of p63-positive and/or KRT5-positive populations in IF staining images ($n = 3$). (**E** to **H**) Genome browser view of p63 CUT&Tag and RNA-seq upon induction of ΔNp63α expression. Note that ΔNp63α directly binds to *KRT5*, *KRT15*, *LAMB3*, and *ITGB4*.

KRT13 (Fig. 6, G and H). Together, these results suggest that ectopic ΔNp63α expression confers squamous cell identity to eNEC cells.

## EZH2i promotes squamous differentiation of eNEC cells through derepressing p63

We next determined whether epigenetic reactivation of ΔNp63α through EZH2i similarly drives the squamous transdifferentiation of eNEC cells. We performed RNA sequencing and qRT-PCR to analyze the gene expression of TYUC-1 cells following EPZ-6438 treatment for 6 days. EZH2i significantly induced the expression of *p63* and squamous marker genes, including *KRT5*, *KRT14*, and *SOX2* (Fig. 7A, fig. S5A, and table S5). Furthermore, gene ontology enrichment analysis revealed that EZH2i promoted the expression of genes that are associated with squamous epithelial cells in tissues like the forestomach and lung (Fig. 7B). This chromatin and transcriptome remodeling was accompanied by increased apoptosis, as shown by the accumulation of cleaved caspase-3 (fig. S5B), as well as decreased cell proliferation (fig. S5C). In addition, EPZ-6438 treatment decreased the frequencies [dimethyl sulfoxide (DMSO), 1.65 ± 0.06%; EPZ-6438, 0.84 ± 0.04%; $P < 0.001$] and sizes of eNEC organoids (DMSO, 192.35 ± 59.14 μm; EPZ-6438, 85.82 ± 19.67 μm; $P < 0.001$) (fig. S5, D to F). We also observed the expression of p63, KRT5, and SOX2 in eNEC organoids treated with EPZ-6438 (Fig. 7, C to E). In contrast, the levels of H3K27me3 and neuroendocrine marker SYP were decreased in $p63^+$ cells (Fig. 7, C and F, and fig. S5A). Overall, p63 was ectopically expressed in 22.7% of organoids upon EZH2i (Fig. 7G), and 73.6% of cells in these organoids expressed p63 (Fig. 7H). To rule out potential off-target effects of drug treatment, we used another EZH2 inhibitor, GSK126, and observed a consistent reduction in the formation efficiency (DMSO, 1.71 ± 0.06%; GSK126, 0.93 ± 0.07%; $P < 0.001$) and size of eNEC organoids (DMSO, 189.76 ± 59.09 μm; GSK126, 94.92 ± 19.67 μm; $P < 0.001$) (fig. S5G). Organoids treated with GSK126 also exhibited increased expression of p63 and KRT5 (fig. S5, H and I). Furthermore, we used two independent short hairpin RNAs (shRNAs) to knock down *EZH2* in TYUC-1 organoids (fig. S6, A and B) and

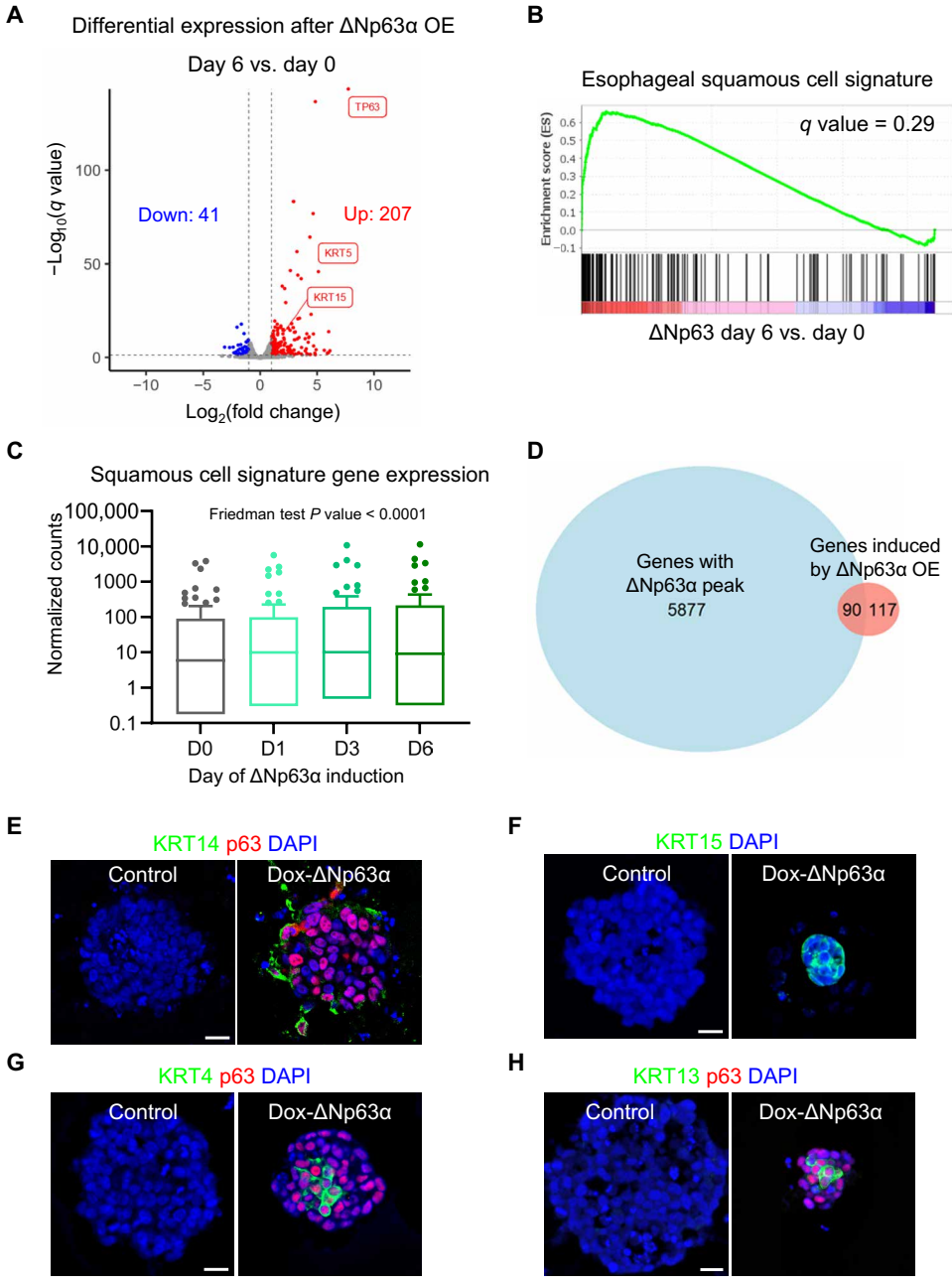


**Fig. 6. ΔNp63 reprograms esophageal neuroendocrine cancer cells into squamous cells.** (**A**) Volcano plot of differentially expressed genes upon induction of ΔNp63α expression by doxycycline for 6 days. $n = 3$ independent experiments. OE, overexpression. (**B**) GSEA analysis showing that the esophageal squamous cell gene signature is positively correlated with ΔNp63α overexpression over time. (**C**) Expression levels of genes of the "Descartes Fetal Stomach Squamous Epithelial Cells" gene set at 0, 1, 3, and 6 days of doxycycline treatment. (**D**) Venn diagram showing the overlap between ΔNp63α-bound genes and ΔNp63α-induced genes. (**E** to **H**) IF staining of p63, KRT14, KRT15, KRT4, and KRT13 in the TYUC-1 tumor organoids with doxycycline-induced overexpression of ΔNp63α (Dox-ΔNp63α) versus the untreated (control). Scale bars, 20 μm.

found that *EZH2* knockdown consistently led to the ectopic expression of p63 and KRT5 (fig. S6C).

Next, we compared EZH2i treatment to ΔNp63α overexpression in their ability to up-regulate squamous identity genes (fig. S6D). We found several genes that were only induced by EZH2i. These EZH2i-specific squamous genes exhibited higher levels of H3K27me3 at associated p63 peaks (fig. S6, E and F). We therefore speculate that, in the context of ΔNp63α overexpression, the presence of H3K27me3 may limit the ability of ΔNp63α to up-regulate a subset of its target genes. EZH2i treatment not only induced p63 expression but also decreased H3K27me3, thus allowing p63 to activate target gene transcription more efficiently. Furthermore, we examined additional known regulators of squamous identity in our datasets and found that *SOX2* and *BMP4* genes were marked by H3K27me3 in TYUC-1

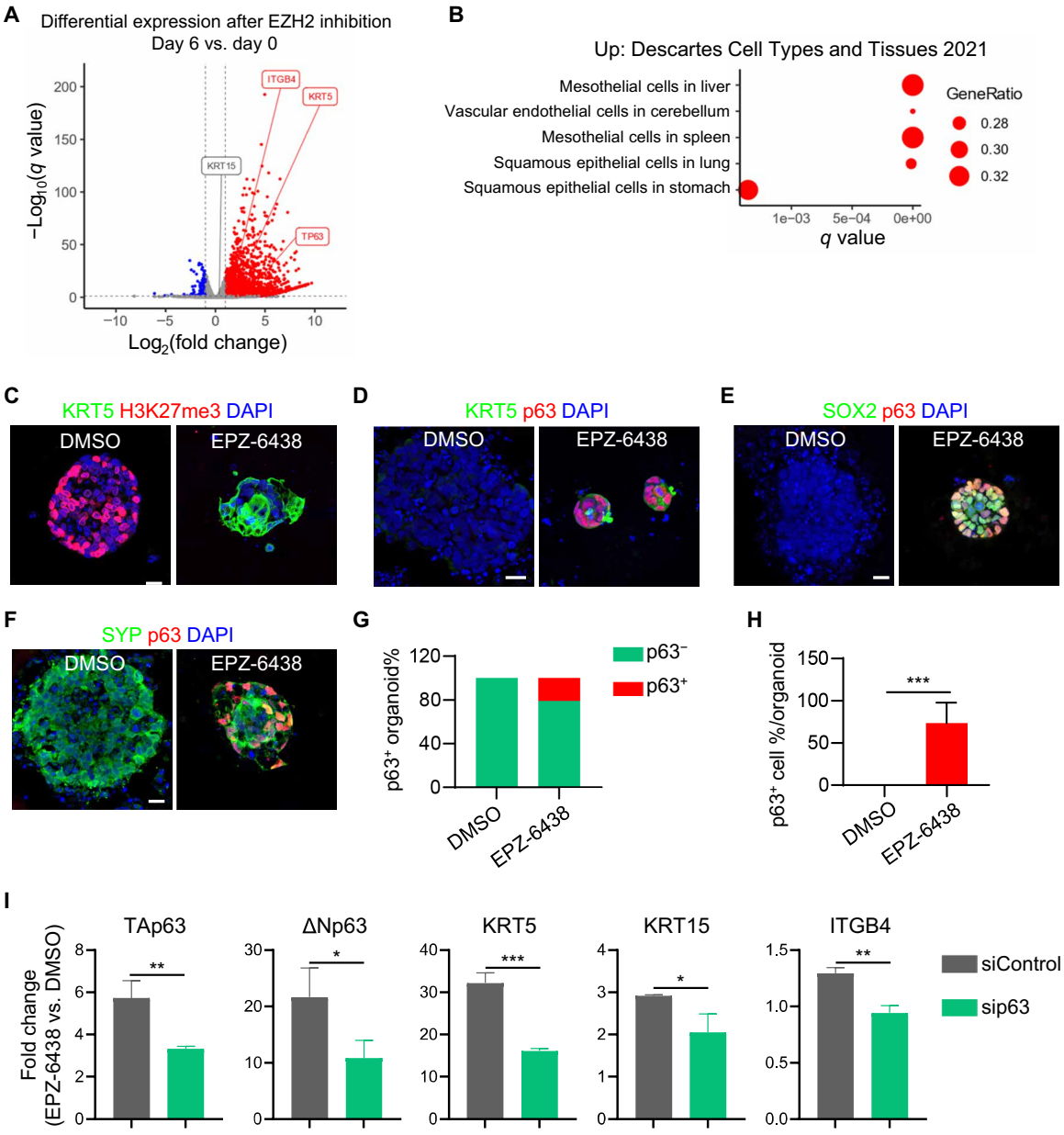


**Fig. 7. EZH2i promotes squamous differentiation of esophageal neuroendocrine cancer organoids through p63.** (**A**) Volcano plot of differentially expressed genes upon treatment of TYUC-1 cells with DMSO or 2 μM EPZ-6438 for 6 days. $n = 3$ independent experiments. (**B**) "Descartes Cell Types and Tissues" gene ontology enrichment analysis of up-regulated genes. (**C** to **F**) IF staining of H3K27me3; basal cell markers p63, KRT5, and SOX2; and the neuroendocrine cell marker SYP in 3D TYUC-1 organoids. (**G** and **H**) Quantification of $p63^+$ organoids (G) and $p63^+$ cells (H) in organoids that contain $p63^+$ cells. ***$P < 0.001$. (**I**) Gene expression fold change (2 μM EPZ-6438 versus DMSO) of TYUC-1 organoids transfected with p63 (sip63) or control (siControl) small interfering RNA (siRNA). *$P < 0.05$, **$P < 0.01$, and ***$P < 0.001$. Scale bars, 20 μm.

cells (fig. S7A) and up-regulated by EZH2i (table S5). Both SOX2 and BMP4 can cooperate with p63 to induce epithelial identity (*44*–*46*), which could explain why EZH2i was more potent in activating squamous marker genes.

Last, to determine whether p63 is critical for the neuroendocrine-to-squamous transdifferentiation following EZH2i, we used small interfering RNA (siRNA) to knock down p63 and observed reduced up-regulation of squamous genes upon EPZ-6438 treatment (Fig. 7I). In agreement with its key role downstream of EZH2i, both p63 isoforms, but not other squamous marker genes, were among the early response genes following EZH2i treatment for just 8 hours (fig. S7B). Furthermore, we found that there were no p63-negative but $KRT5^+$ cell populations in EZH2i-treated organoids (fig. S7C). Together, these results confirm that EZH2 epigenetically suppresses the expression of p63 in eNECs and that p63 plays a major role in the transition between squamous and neuroendocrine cell identities following EZH2i.

## DISCUSSION

Cell fate determination is critical for tissue development and cancer progression. Here, we demonstrated that p63 is a critical regulator of the switch between squamous and neuroendocrine lineages in the esophagus. *p63* deletion promotes the differentiation of both mouse and human esophageal progenitor cells into neuroendocrine cells. Conversely, ectopic ΔNp63α expression promotes the squamous differentiation of eNEC cells by directly binding to the squamous genes. Our study further revealed that p63 is epigenetically silenced by EZH2-mediated H3K27me3, which is accompanied by a reduction in H3K27ac levels. Treatment with EZH2 inhibitors leads to p63 expression and promotes the squamous differentiation of eNECs. These results suggest that the lineage gatekeeping function of p63 is repressed by eNECs to maintain the neuroendocrine identity and represents a potential target for epigenetic therapies.

p63 is a master regulator of basal cells, and ablation of *p63* leads to failed stratification of the epithelium in the developing esophagus (*13*). We showed here that p63 not only regulates the generation of the stratified epithelium but also actively blocks non-squamous cell fate. These functionalities are conserved in hEPCs. The *p63* gene uses two different promoters to generate two major isoforms (*41*). Our findings indicate that ΔNp63α plays a more prominent role than TAp63α in promoting squamous cell fate in eNEC. In line with this, ΔNp63α overexpression promotes squamous differentiation of eNEC cells. Conversely, ΔNp63α knockdown blocks the squamous differentiation of eNECs induced by EZH2i. $p63^+$ basal cells are also abundantly present in the prostate, where transdifferentiation toward neuroendocrine carcinoma occurs (*47*). Whether p63 plays a broader role in governing the shuttle between squamous and neuroendocrine cell fates in other tissues remains to be addressed.

The cell of origin for eNEC is not clear. Neuroendocrine cells are considered the major cell of origin for SCLCs (*48*, *49*). Merkel cells are found in the middle portion of the human esophagus (*27*), and a clinical study revealed that eNEC arises primarily in the middle or lower third of the esophagus (*50*). However, the presence of Merkel cells in the esophagus of other species, including rodents, remains unknown. We previously reported that, during esophageal-tracheal separation, a subpopulation of epithelial progenitor cells originating from the trachea and lung translocate and incorporate into the esophagus as $p63^+$ basal cells (*51*). It will be interesting to determine whether these cells of respiratory origin contribute to the formation of eNEC. Notably, the mutational and copy number variation signatures of eNEC are more similar to ESCC than SCLC (*52*), suggesting a possible common origin of eNEC and ESCC. In addition, eNEC was reported to arise from ESCC following combined treatment with chemotherapy and radiotherapy (*9*). Our study favors basal/squamous cells or their progenitors as one of the cells of origin for eNEC. Our findings further suggest that silencing of p63 likely represents a critical step in the squamous-to-neuroendocrine conversion during tumor progression. Such a lineage transition seems reversible. Ectopic ΔNp63α expression was able to bind and activate squamous genes in eNEC cells. Thus, epigenetic regulation of p63 expression could be key to the lineage plasticity that underlies esophageal intra-tumoral heterogeneity and enables cancer cells to adapt to niche- and drug-induced stressful environments.

eNEC is rare yet extremely aggressive, with high metastatic potential and a poor prognosis (*29*). No standard therapy has been established for eNEC. Chemo- and radiation therapies approved for ESCC have proven to be largely ineffective against eNEC. Furthermore, recent multiomics profiling reveals that, unlike ESCC, eNEC is poorly immune infiltrated, suggesting that it is a poor candidate for immune checkpoint inhibitors (*32*). Our experiments indicate that several epigenetic inhibitors, including the FDA-approved EZH2 and HDAC inhibitors, robustly activate the squamous gene expression program in eNEC. Our results suggest that this is predominantly through the derepression of p63; however, we cannot rule out the activity of other EZH2-regulated genes in this process, such as BMP4 and SOX2. We observed a modest yet significant effect of EZH2i on the proliferation of eNEC organoids. Future studies are needed to assess the impact of EZH2 inhibitors and other epigenetic therapies on the squamous transdifferentiation and growth of eNEC tumors in vivo. We propose that the switch to a squamous cell state by EZH2 inhibitors may sensitize eNEC to chemotherapy, targeted therapy, and immunotherapy approved for ESCC, and these combination treatment strategies warrant further investigations in preclinical and clinical studies.

In summary, we identified an important role of p63 in repressing the differentiation of esophageal progenitor cells into neuroendocrine cells in mouse models and hESCs. Ectopic p63 expression is sufficient to promote the transdifferentiation of eNECs toward squamous cells. We further showed that p63 is silenced via EZH2-mediated H3K27me3 epigenetic modification in eNEC cells. Accordingly, EZH2i is sufficient to activate p63, which orchestrates squamous gene expression in eNEC cells. Therefore, our findings identify an important regulatory mechanism by the EZH2-p63 axis in determining squamous versus neuroendocrine cell fates during normal esophageal development and tumor lineage plasticity.

## MATERIALS AND METHODS

### Mice

$p63^{CreERT2}$ (*53*) mice were maintained on a C57BL/6 and 129SvEv mixed background. Mice were maintained in the animal facilities of Columbia University under a 12-hour light/12-hour dark cycle. Both sexes were used. All animal experiments were conducted according to the procedures approved by the Columbia University Institutional Animal Care and Use Committee (approval protocol number AC-AABM6565).

### Clinical samples

Human esophageal small cell carcinoma samples were collected from The First Affiliated Hospital of Xi'an Jiaotong University, Xi'an, Shaanxi, China. This study was approved by the ethics commissions of the participating hospitals with written informed consent from the patients.

### hESC culture

*p63 KO* H9 cell lines were originally generated by A. Oro lab at Stanford University (*45*). H9 hESCs were maintained on mitotically arrested mouse embryonic fibroblast feeder cells in the medium composed of 80 ml of Dulbecco's Modified Eagle's Medium (DMEM)/F1, 20 ml of KnockOut Serum Replacement, 1 ml of GlutaMAX, 1 ml of minimum essential medium nonessential amino acids solution, 0.7 μl of 2-mercaptoethanol, 0.2 ml of primocin, and fibroblast growth factor2 (FGF2; 20 ng/ml). Cells were maintained in an incubator of 5% $CO_2$ at 37°C. hESC research was conducted under the approval of the Columbia University Human Embryonic and Human Embryonic Stem Research Committee.

### hESC differentiation into esophageal epithelial cells and organoids

We have reported a detailed protocol for esophageal differentiation of hESCs (*39*, *40*). Serum-free differentiation (SFD) medium was prepared as following: 150 ml of Iscove's Modified Dulbecco's Medium medium, 50 ml of F12, 1.5 ml of 7.5% Bovine Albumin Fraction V Solution, 2 ml of GlutaMAX, 1 ml of $N_2$, 2 ml of B27, 2 ml of penicillin/streptomycin, L-ascorbic acid (50 μg/ml), and 1-thioglycerol (0.04 μl/ml). hESCs were differentiated into endodermal spheroids in SFD medium with activin A (100 ng/ml), BMP2 (0.5 ng/ml), FGF2 (2.5 ng/ml), and 10 nM Y-27632 for 72 hours in six-well low-attachment plates. Endoderm spheroids were disassociated into single cells and replated in fibronectin-coated 24-well plates and induced into foregut endoderm epithelial cells with Noggin (100 ng/ml) and 10 mM SB431542 for 48 hours. To induce esophageal specification, cells were continued to be cultured in Noggin (100 ng/ml) and 10 mM SB431542 and epidermal growth factor (EGF; 100 ng/ml) for 4 days and EGF (100 ng/ml) for another 14 days. Esophageal epithelial cells were then subjected to IF staining and qRT-PCR analysis. For esophageal organoid establishment, we embedded endodermal spheroids in Matrigel and cultured the organoids with SFD medium supplemented with Noggin (100 ng/ml), 10 mM SB431542, and EGF (100 ng/ml) until day 53. Organoids were then harvested for immunostaining analysis.

### TYUC-1 cell culture and tumor organoid culture

TYUC-1 (JCRB1512, Japanese Collection of Research Biosources Cell Bank) is an eNEC cell line that was originally established from a patient with esophageal small cell carcinoma (*54*). The cell line was maintained in DMEM/F12 (Corning) and 10% serum and 1% penicillin/streptomycin in suspension culture. To establish 3D tumor organoids, TYUC-1 cells were digested with 0.05% trypsin-EDTA at 37°C for 15 min and disassociated with P1000 pipettes into single cells. A total of 20,000 cells in 100 μl of medium were then mixed with 100 μl of Matrigel (Corning) and added to the 24-well inserts. Matrigel-embedded cells were allowed to solidify in a cell culture incubator at 37°C for 30 min before medium was added. The organoid culture medium contained DMEM/F12 supplemented with 10% serum and 1% penicillin/streptomycin. Medium was refreshed every other day. To inhibit EZH2 activity, TYUC-1 cells or organoids were treated with either 2 μM EPZ-6438 or 2 μM GSK126 with DMSO as vehicle control.

### EZH2 shRNA lentivirus generation

To knockdown *EZH2*, two shRNAs targeting *EZH2* (shEZH2-a: CCGGCCCAACATAGATGGACCAAATCTCGAGATTTGGTCCATCTATGTTGGGTTTTTG and shEZH2-b: CCGG CGGAAATCTTAAACCAAGAATCTCGAGATTCTTGGTTTAA GA TTTC CG TTTTTG) were designed and cloned into the pLKO.1 vector (Addgene, plasmid no. 10879) according to the method by Moffat *et al.* (*55*). The control shRNA sequence was CCTAAGGTTAAGTCGCCCTCGCTCGAGCGAGGGCGACTTAACCTTAGG. Plasmids were amplified in *Escherichia coli DH*5α and isolated using the QIAGEN QIAprep Spin Miniprep Kit (QIAGEN) according to the manufacturer's instructions. Lentivirus was produced with the packaging plasmids psPAX2 (Addgene, plasmid no. 12260) and pMD2.G (Addgene, plasmid no. 12259) in 293 T cells. TransIT (Mirus) was used to transfect the plasmids. TYUC-1 cells cultured in suspension were infected with lentivirus, and 1 μM polybrene was added to improve the infecting efficiency. Cells were collected 24 hours later and resuspended for organoid culture, as mentioned above. To knock down human *TP63*, siRNA targeting human *TP63* (ON-TARGETplus, catalog no. L-003330-00-0005) and control siRNA (ON-TARGETplus, catalog no. D-001810-10-05) were used. siRNAs were transfected with Lipofectamine RNAiMAX (Thermo Fisher Scientific).

### Overexpression of TAp63 and ΔNp63 in TYUC-1 cells

The coding sequence of *TAp63* and Δ*Np63* was amplified with high-fidelity Taq polymerase using primers TAp63-EX-F: gaataccggtgcgctgccaccATGAATTTTGAAACTTCACGGTGTGCC and TAp63-EX-R: cgggatccCTCCCCCTCCTCTTTGATGC, ΔNp63-EX-F: gaataccggtctagagctgccaccATGGGCTCCGGCTCCTTGTACCTGGAAAACAATGCC, and TAp63-EX-R. PCR products were digested with Age I and Bam HI and cloned into the Tet-on plasmid TLCV2 (Addgene, plasmid no. 87360) digested with the same enzymes. Lentivirus was packaged with the plasmids psPAX2 and pMD2.G in 293 T cells. TYUC-1 cells were infected with lentivirus containing *TAp63* or Δ*Np63*, with the original empty vector plasmid as a control. Infected cells were maintained in the culture medium supplemented with puromycin (1 μg/ml).

### Immunostaining

Antigen retrieval on tissue slides was performed using an antigen unmasking solution (Vector Laboratories, no. H-3301-250). Cells were fixed with 4% paraformaldehyde in 1× phosphate-buffered saline (PBS) for 10 min. Tissues or cells were treated with a blocking solution composed of 1× PBS with 3% donkey serum and 0.3% Triton X-100 for 30 min. Primary antibodies diluted in blocking solution were added to the top of tissue slides and cells and incubated at 4°C overnight. The next day, tissues and cells were washed with 1× PBS three times before fluorophore-tagged secondary antibodies were added and incubated at room temperature for 2 hours. Tissues and cells were washed with 1× PBS three times. Tissue slides were mounted with 4′,6-diamidino-2-phenylindole–containing mounting medium (SouthernBiotech, no. 0100-20). Antibodies are summarized in table S6. Images were taken by a Lecia DMi8 (Leica Microsystems) or LSM 700 laser scanning confocal microscope (Carl Zeiss). Representative images were generated by individually scanned images stitched with Leica Application Suite X software (Leica Microsystems) or Zen software (Carl Zeiss). Quantification of cell populations was performed manually using ImageJ (v1.54f) (>100 cells per condition were counted), and signal intensity was measured using CellProfiler (v4.2.6).

### RNA sequencing

The epithelium was isolated from the esophagus of E12.5 *p63 KO* ($p63^{CreERT2/CreERT2}$ homozygous) mutants and littermate controls, and RNA was purified with the PicoPure RNA Isolation Kit (Thermo Fisher Scientific). We determined RNA concentration with the 2100 Bio-analyzer (Agilent Technologies) and then used an Illumina TruSeq RNA prep kit (Illumina) to establish libraries, which were sequenced with the Illumina HiSeq400. Samples were multiplexed in each lane, which yielded a targeted number of single-end/pair-end 100–base pair (bp) reads for each sample, as a fraction of 180 million reads for the whole lane. Real-Time Analysis (Illumina) was used for base calling and bcl2fastq (version 1.8.4) for converting binary base call to fastq format, coupled with adaptor trimming. We mapped the reads to a reference genome (Mouse: UCSC/mm9) using Tophat

(version 2.1.0) with four mismatches (--read-mismatches = 4) and 10 maximum multiple hits (--max-multihits= 10). The expression levels of each gene were presented as fragments per kilobase of transcript per million mapped reads in this study. For RNA sequencing of TYUC-1 cells, total RNA was extracted in TRIzol (Invitrogen) and precipitated in ethanol (DECON Labs). For RNA sequencing of doxycycline-treated cells for induction of TAp63 and ΔNp63 expression, libraries were prepared using the NEBNext Ultra kit [New England Biolabs (NEB), nos. E7490, E7770, E7335, and E7500] and sequenced using a Nextseq500/550 sequencer. Paired-end reads were obtained and mapped to the human genome assembly hg38 using HISAT2 (v2.1.0). The mapped read count of each gene was measured by featureCounts (v1.6.1). For RNA sequencing of EPZ-6438–treated cells, RNA samples were submitted to the Columbia University Genome Center for library preparation, sequencing, and bioinformatic analysis. For both experiments, differential gene expression was calculated by the R package DESeq2 (v1.28.0), and GSEA was performed using GSEA software (v4.1.0) (*56*). Visualization was done using the ggplot2 R package.

### Single-cell RNA sequencing

Esophageal tissues were isolated from E18.5 mouse embryos, and muscle layers were removed using forceps. Mesenchyme was removed after incubation with dispase for 5 min at room temperature. The epithelium was then digested with 0.1% trypsin for 10 min at 37°C into single cells. Single-cell sequencing libraries were generated using the Single Cell 3′ reagent kit v2 (10x Genomics) and sequenced by the Illumina NovaSeq 6000 instrument. Raw sequencing data were processed by the Cell Ranger R package (version 7.1.0). The filtered data were analyzed using the Seurat package (version 5.0.1) in R (version 4.3.1). WT cells with >500 and <8000 genes, >10 and <50,000 RNA counts, and <15% mitochondrial transcripts and p63 KO cells with >500 and <10,000 genes, >10 and <100,000 RNA counts, and <15% mitochondrial transcripts were selected for further analysis. Datasets were normalized using the standard parameters, and 2000 highly variable genes were selected. FindIntegrationAnchors and IntegrateData functions were used to integrate data to correct batch effects, followed by scaling with the ScaleData function. Principal components analysis was then performed on the scaled data, with 15 principal components selected for clustering at a resolution of 0.4. Epithelial cells were selected on the basis of the high expression of Epcam and Cdh1. Subsequently, we annotated cells with cell-specific genes: basal cells (Trp63, Krt5, and Krt14), proliferating cells (Mki67), suprabasal cells (Krt4, Krt13, and Lor), neuroendocrine cells (Syp, Insm1, and Chga), and ciliated cells (Foxj1 and Ccdc17). The single-cell trajectory analysis was conducted using Monocle (version 2.28.0).

### Quantitative real-time polymerase chain reaction

We used TRIzol to lyse cells or tissues and purified the RNA with the RNeasy Mini Kit (QIAGEN). Reverse transcription was performed using the SuperScript III First-Strand SuperMix (Invitrogen). cDNA abundance was measured by RT-PCR using the iQ SYBR Green and StepOnePlus RT-PCR System (Applied Biosystems). The transcript levels of each gene were normalized to β-actin or glyceraldehyde-3-phosphate dehydrogenase. Primer sequences are summarized in table S7.

### Cleavage under targets and tagmentation

CUT&Tag was performed as described previously (*57*). In brief, $2 \times 10^5$ cells were washed once with 1 ml of wash buffer [20 mM Hepes (pH 7.5), 150 mM NaCl, 0.5 mM spermidine (Sigma-Aldrich), and 1× protease inhibitor cocktail (Roche)]. Concanavalin A–coated magnetic beads (Bangs Laboratories) were washed twice with binding buffer [20 mM Hepes (pH 7.5), 10 mM KCl, 1 mM $MnCl_2$, and 1 mM $CaCl_2$]. Beads (10 μl per sample) were added to cells in 400 μl of wash buffer and incubated at room temperature for 15 min. Bead-bound cells were resuspended in 100 μl of antibody buffer [20 mM Hepes (pH 7.5), 150 mM NaCl, 0.5 mM spermidine, 0.06% digitonin (Sigma-Aldrich), 2 mM EDTA, 0.1% bovine serum albumin, and 1× protease inhibitor cocktail] and incubated with H3K27me3 antibody (Cell Signaling Technology, no. 9733), H3K27ac antibody (Active Motif, no. 39134), BRD4 antibody (Epicypher, no. 13-2003), or normal rabbit immunoglobulin G (Cell Signaling Technology, no. 2729) at 4°C overnight on nutator. After being washed once with Dig-wash buffer [20 mM Hepes (pH 7.5), 150 mM NaCl, 0.5 mM spermidine, 0.05% digitonin, and 1× protease inhibitor cocktail], bead-bound cells were incubated with 1 μl of guinea pig anti-rabbit secondary antibody (Antibodies Online, ABIN101961) and 2 μl of hyperactive pA-Tn5 transposase adapter complex in 100 μl of Dig-300 buffer [20 mM Hepes-NaOH (pH 7.5), 0.5 mM spermidine, 1× protease inhibitor cocktail, 300 mM NaCl, and 0.01% digitonin] at room temperature for 1 hour. Cells were washed three times with Dig-300 buffer to remove unbound antibody and Tn5 and then resuspended in 300 μl of tagmentation buffer (10 mM $MgCl_2$ in Dig-300 buffer) and incubated at 37°C for 1 hour. Ten microliters of 0.5 M EDTA, 3 μl of 10% SDS, and 5 μl of proteinase K (10 mg $ml^{-1}$) were added to each sample and incubated at 50°C for 1 hour to terminate tagmentation. DNA was purified using chloroform isoamyl alcohol (Sigma-Aldrich) and eluted with 25 μl of $ddH_2O$. For library amplification, 21 μl of DNA was mixed with 2 μl of i5 unique index primer (10 μM), 2 μl of i7 unique index primer (10 μM), and 25 μl of NEBNext High-Fidelity 2X PCR Master Mix (NEB) and subjected to the following PCR program: 72°C, 5 min; 98°C, 30 s; 13 cycles of 98°C, 10 s and 63°C, 10 s; 72°C, 1 min; and hold at 10°C. To purify the PCR products, 1.1× volumes of pre-warmed Ampure XP beads (Beckman Coulter) were added and incubated at room temperature for 10 min. Libraries were washed twice with 80% ethanol and eluted in 20 μl of 10 mM tris-HCl (pH 8). Libraries were sequenced on a NextSeq 550 platform (Illumina, 75 cycles, High Output Kit v2.0) and 75-bp paired-end reads were generated. For H3K27me3 and H3K27ac, 2 μl of SNAP-ChIP K-MetStat panel and K-AcylStat panel nucleosomes (EpiCypher), respectively, were added as spike-in controls at the primary antibody incubation step. H3K27ac and BRD4 CUT&Tag were initially lightly fixed with 0.1% paraformaldehyde for 5 min and neutralized by 125 mM glycine to preserve target stability.

### CUT&Tag data analysis

CUT&Tag reads of TYUC-1 cell samples were mapped to the mouse human assembly hg38 using Bowtie2 (v2.3.5.1, parameters: --local --very-sensitive-local --no-unal --no-mixed --no-discordant --phred33 -I 10 -X 700). Potential PCR duplicates were removed by the function "MarkDuplicates" (parameter: REMOVE_DUPLICATES = true) of Picard (v2.24.2). Genomic enrichments of CUT&Tag signals were generated using deepTools (v3.3.2, parameters

bamCoverage --normalizeUsing CPM --binSize 25 --smoothLength 100 --scaleFactor 1). Peaks were called using MACS2 and annotated by the R package ChIPSeeker (v1.28.3). Known motif enrichment analysis was performed using HOMER (v4.11). For H3K27me3 and H3K27ac, the number of reads for each barcode was counted to determine the scaling factor. Tracks were visualized using Integrative Genomics Viewer (IGV). Read counts of H3K27me3 and p63 CUT&Tag data in genomic elements were measured by featureCounts (v2.0.0). For visualization, we used the R package ggplot2 (v3.3.2) and GraphPad Prism software v9.

### ChIP-seq assay and data analysis

For native ChIP $2 \times 10^7$ cells were resuspended in digestion buffer [50 mM tris (pH 7.6), 1 mM $CaCl_2$, 0.2% Triton X-100, and 1× protease inhibitor cocktail] with micrococcal nuclease (Sigma-Aldrich) to generate mainly mononucleosomes with a minor fraction of dinucleosomes for histone modification mapping. The reaction was stopped using a final concentration of 5 mM EDTA. Samples were sonicated for three cycles of 20 s on/20 ss off at high amplitude in ice water. Then, samples were dialyzed using a 3500 molecular weight membrane against 400 ml of radioimmunoprecipitation assay (RIPA) buffer [10 mM tris (pH 7.6), 1 mM EDTA, 0.1% SDS, 0.1% Na-Deoxycholate, and 1% Triton X-100]. Samples were centrifuged at 10,000 rpm for 10 min at 4°C, and supernatants were used for fragment size evaluation and immunoprecipitation. Primary antibody against H3K27me3 (table S6) was bound to 150 μl of Protein A Dynabeads (Invitrogen) in 1× PBS and 0.01% Tween overnight at 4°C. Antibody-bound bead mix (70 μl) was added to 860 μl of chromatin extract and rotated overnight at 4°C. Beads were washed thrice with RIPA buffer, twice with RIPA buffer and 0.3 M NaCl, twice with LiCl buffer (0.25 M LiCl, 0.5% NP-40, and 0.5% Na-deoxycholate), and once with Tris-EDTA buffer and 50 mM NaCl. Then, 210 μl of elution buffer [50 mM tris-HCl (pH 8.0), 10 mM EDTA, and 1% SDS] is added, and samples are shaken for 30 min at 65°C. After centrifugation (1 min, 16,000*g* at room temperature), supernatants are treated with proteinase K (Roche) for 2 hours at 55°C. DNA was purified using the QIAGEN DNA Purification Kit according to the manufacturer's instructions. Libraries were prepared using the NEBNext Ultra II DNA Library Prep Kit for Illumina according to the manufacturer's instructions, and single-end 75-bp reads were obtained using an Illumina NextSeq 500 sequencer. ChIP-seq reads were mapped to the human genome assembly hg38 using HISAT2 (v2.1.0, default parameters). Genomic enrichments of CUT&Tag signals were generated using deepTools (v3.3.2). Tracks were visualized using IGV.

### Chromatin chemical probe screen

For the chromatin chemical probe screening, $5 \times 10^5$ TYUC-1 cells were plated and treated with EPZ-6438 (2 μM), Vorinostat (1 μM), romidepsin (1 nM), JQ1 (500 nM), Seclidemstat (500 nM), EPZ5676 (10 μM), UNC0638 (1 μM), A485 (250 nM), MG149 (10 μM), PRT4165 (10 μM), or DMSO. Medium was refreshed every 2 days.

### Quantification and statistical analysis

The data were presented as the means ± SD using GraphPad Prism software. Statistical significance was determined by the Student's *t* test. At least three biological replicates were included. *P* values of 0.05 or less were considered to be statistically significant.

## Supplementary Materials

**The PDF file includes:**
Figs. S1 to S7
Legends for tables S1 to S7

**Other Supplementary Material for this manuscript includes the following:**
Tables S1 to S7

## REFERENCES AND NOTES


1. M. Jabbari, C. A. Goresky, J. Lough, C. Yaffe, D. Daly, C. Cote, The inlet patch: Heterotopic gastric mucosa in the upper esophagus. *Gastroenterology* **89**, 352–356 (1985).
2. S. J. Spechler, J. M. Zeroogian, D. A. Antonioli, H. H. Wang, R. K. Goyal, Prevalence of metaplasia at the gastro-oesophageal junction. *Lancet* **344**, 1533–1536 (1994).
3. M. Jiang, H. Li, Y. Zhang, Y. Yang, R. Lu, K. Liu, S. Lin, X. Lan, H. Wang, H. Wu, J. Zhu, Z. Zhou, J. Xu, D. K. Lee, L. Zhang, Y. C. Lee, J. Yuan, J. A. Abrams, T. C. Wang, A. R. Sepulveda, Q. Wu, H. Chen, X. Sun, J. She, X. Chen, J. Que, Transitional basal cells at the squamous-columnar junction generate Barrett's oesophagus. *Nature* **550**, 529–533 (2017).
4. M. Quante, G. Bhagat, J. A. Abrams, F. Marache, P. Good, M. D. Lee, Y. Lee, R. Friedman, S. Asfaha, Z. Dubeykovskaya, U. Mahmood, J. L. Figueiredo, J. Kitajewski, C. Shawber, C. J. Lightdale, A. K. Rustgi, T. C. Wang, Bile acid and inflammation activate gastric cardia stem cells in a mouse model of Barrett-like metaplasia. *Cancer Cell* **21**, 36–51 (2012).
5. K. G. Braslis, R. C. David, E. Nelson, F. Civantos, M. S. Soloway, Squamous cell carcinoma of the prostate: A transformation from adenocarcinoma after the use of a luteinizing hormone-releasing hormone agonist and flutamide. *Urology* **45**, 329–331 (1995).
6. J. Lee, Transformation of adenocarcinoma of prostate to squamous cell carcinoma following hormonal treatment: A case report and review of the literature. *Radiol. Case Rep.* **14**, 483–489 (2019).
7. M. Zou, R. Toivanen, A. Mitrofanova, N. Floch, S. Hayati, Y. Sun, C. Le Magnen, D. Chester, E. A. Mostaghel, A. Califano, M. A. Rubin, M. M. Shen, C. Abate-Shen, Transdifferentiation as a mechanism of treatment resistance in a mouse model of castration-resistant prostate cancer. *Cancer Discov.* **7**, 736–749 (2017).
8. J. Shia, S. K. Tickoo, J. G. Guillem, J. Qin, A. Nissan, A. Hoos, A. Stojadinovic, L. Ruo, W. D. Wong, P. B. Paty, M. R. Weiser, B. D. Minsky, D. S. Klimstra, Increased endocrine cells in treated rectal adenocarcinomas: A possible reflection of endocrine differentiation in tumor cells induced by chemotherapy and radiotherapy. *Am. J. Surg. Pathol.* **26**, 863–872 (2002).
9. M. Morita, H. Saeki, Y. U. Nakaji, Y. Zaitsu, M. Hirahashi, T. Ohguri, E. Oki, Y. Toh, Y. Oda, Y. Maehara, Conversion to neuroendocrine carcinoma from squamous cell carcinoma of the esophagus after definitive chemoradiotherapy. *Anticancer Res.* **36**, 4045–4049 (2016).
10. Y. Zhang, D. Bailey, P. Yang, E. Kim, J. Que, The development and stem cells of the esophagus. *Development* **148**, dev193839 (2021).
11. Y. Zhang, M. Jiang, E. Kim, S. Lin, K. Liu, X. Lan, J. Que, Development and stem cells of the esophagus. *Semin. Cell Dev. Biol.* **66**, 25–35 (2017).
12. P. Rodriguez, S. Da Silva, L. Oxburgh, F. Wang, B. L. Hogan, J. Que, BMP signaling in the development of the mouse esophagus and forestomach. *Development* **137**, 4171–4176 (2010).
13. Y. Daniely, G. Liao, D. Dixon, R. I. Linnoila, A. Lori, S. H. Randell, M. Oren, A. M. Jetten, Critical role of p63 in the development of a normal esophageal and tracheobronchial epithelium. *Am. J. Physiol. Cell Physiol.* **287**, C171–C181 (2004).
14. A. Yang, R. Schweitzer, D. Sun, M. Kaghad, N. Walker, R. T. Bronson, C. Tabin, A. Sharpe, D. Caput, C. Crum, F. McKeon, p63 is essential for regenerative proliferation in limb, craniofacial and epithelial development. *Nature* **398**, 714–718 (1999).
15. A. A. Mills, B. Zheng, X. J. Wang, H. Vogel, D. R. Roop, A. Bradley, p63 is a p53 homologue required for limb and epidermal morphogenesis. *Nature* **398**, 708–713 (1999).
16. M. I. Koster, D. Dai, B. Marinari, Y. Sano, A. Costanzo, M. Karin, D. R. Roop, p63 induces key target genes required for epidermal morphogenesis. *Proc. Natl. Acad. Sci. U.S.A.* **104**, 3255–3260 (2007).
17. D. Chakravarti, X. Su, M. S. Cho, N. H. Bui, C. Coarfa, A. Venkatanarayan, A. L. Benham, R. E. Flores Gonzalez, J. Alana, W. Xiao, M. L. Leung, H. Vin, I. L. Chan, A. Aquino, N. Muller, H. Wang, A. J. Cooney, J. Parker-Thornburg, K. Y. Tsai, P. H. Gunaratne, E. R. Flores, Induced multipotency in adult keratinocytes through down-regulation of ΔNp63 or DGCR8. *Proc. Natl. Acad. Sci. U.S.A.* **111**, E572–E581 (2014).
18. A. N. Mardaryev, B. Liu, V. Rapisarda, K. Poterlowicz, I. Malashchuk, J. Rudolf, A. A. Sharov, C. A. Jahoda, M. Y. Fessing, S. A. Benitah, G. L. Xu, V. A. Botchkarev, Cbx4 maintains the epithelial lineage identity and cell proliferation in the developing stratified epithelium. *J. Cell Biol.* **212**, 77–89 (2016).
19. E. Soares, H. Zhou, Master regulatory role of p63 in epidermal development and disease. *Cell. Mol. Life Sci.* **75**, 1179–1190 (2018).
20. L. Rinaldi, D. Datta, J. Serrat, L. Morey, G. Solanas, A. Avgustinova, E. Blanco, J. I. Pons, D. Matallanas, A. Von Kriegsheim, L. Di Croce, S. A. Benitah, Dnmt3a and Dnmt3b

associate with enhancers to regulate human epidermal stem cell homeostasis. *Cell Stem Cell* **19**, 491–501 (2016).
21. T. Kurita, R. T. Medina, A. A. Mills, G. R. Cunha, Role of p63 and basal cells in the prostate. *Development* **131**, 4955–4964 (2004).
22. S. Signoretti, D. Waltregny, J. Dilks, B. Isaac, D. Lin, L. Garraway, A. Yang, R. Montironi, F. McKeon, M. Loda, p63 is a prostate basal cell marker and is required for prostate development. *Am. J. Pathol.* **157**, 1769–1775 (2000).
23. X. Wang, H. Ouyang, Y. Yamamoto, P. A. Kumar, T. S. Wei, R. Dagher, M. Vincent, X. Lu, A. M. Bellizzi, K. Y. Ho, C. P. Crum, W. Xian, F. McKeon, Residual embryonic cells as precursors of a Barrett's-like metaplasia. *Cell* **145**, 1023–1035 (2011).
24. C. S. Kuo, M. A. Krasnow, Formation of a neurosensory organ by epithelial cell slithering. *Cell* **163**, 394–405 (2015).
25. K. L. Sinagoga, H. A. McCauley, J. O. Munera, N. A. Reynolds, J. R. Enriquez, C. Watson, H. C. Yang, M. A. Helmrath, J. M. Wells, Deriving functional human enteroendocrine cells from pluripotent stem cells. *Development* **145**, dev165795 (2018).
26. K. Branchfield, L. Nantie, J. M. Verheyden, P. Sui, M. D. Wienhold, X. Sun, Pulmonary neuroendocrine cells function as airway sensors to control lung immune response. *Science* **351**, 707–710 (2016).
27. J. L. Harmse, F. A. Carey, A. R. Baird, S. R. Craig, K. N. Christie, D. Hopwood, J. Lucocq, Merkel cells in the human oesophagus. *J. Pathol.* **189**, 176–179 (1999).
28. A. Ji, R. Jin, R. Zhang, H. Li, Primary small cell carcinoma of the esophagus: Progression in the last decade. *Ann. Transl. Med.* **8**, 502 (2020).
29. J. P. Yun, M. F. Zhang, J. H. Hou, Q. H. Tian, J. Fu, X. M. Liang, Q. L. Wu, T. H. Rong, Primary small cell carcinoma of the esophagus: Clinicopathological and immunohistochemical features of 21 cases. *BMC Cancer* **7**, 38 (2007).
30. J. P. van Meerbeeck, D. A. Fennell, D. K. M. De Ruysscher, Small-cell lung cancer. *Lancet* **378**, 1741–1755 (2011).
31. A. Egashira, M. Morita, R. Kumagai, K. I. Taguchi, M. Ueda, S. Yamaguchi, M. Yamamoto, K. Minami, Y. Ikeda, Y. Toh, Neuroendocrine carcinoma of the esophagus: Clinicopathological and immunohistochemical features of 14 cases. *PLOS One* **12**, e0173501 (2017).
32. R. Li, Z. Yang, F. Shao, H. Cheng, Y. Wen, S. Sun, W. Guo, Z. Li, F. Zhang, L. Xue, N. Bi, J. Wang, Y. Sun, Y. Li, F. Tan, Q. Xue, S. Gao, S. Shi, Y. Gao, J. He, Multi-omics profiling of primary small cell carcinoma of the esophagus reveals RB1 disruption and additional molecular subtypes. *Nat. Commun.* **12**, 3785 (2021).
33. A. Sparmann, M. van Lohuizen, Polycomb silencers control cell fate, development and cancer. *Nat. Rev. Cancer* **6**, 846–856 (2006).
34. S. U. Kass, D. Pruss, A. P. Wolffe, How does DNA methylation repress transcription? *Trends Genet.* **13**, 444–449 (1997).
35. Z. Wang, C. Zang, K. Cui, D. E. Schones, A. Barski, W. Peng, K. Zhao, Genome-wide mapping of HATs and HDACs reveals distinct functions in active and inactive genes. *Cell* **138**, 1019–1031 (2009).
36. K. Struhl, Histone acetylation and transcriptional regulatory mechanisms. *Genes Dev.* **12**, 599–606 (1998).
37. J. Shi, C. R. Vakoc, The mechanisms behind the therapeutic activity of bet bromodomain inhibition. *Mol. Cell* **54**, 728–736 (2014).
38. M. P. Creyghton, A. W. Cheng, G. G. Welstead, T. Kooistra, B. W. Carey, E. J. Steine, J. Hanna, M. A. Lodato, G. M. Frampton, P. A. Sharp, L. A. Boyer, R. A. Young, R. Jaenisch, Histone H3K27ac separates active from poised enhancers and predicts developmental state. *Proc. Natl. Acad. Sci. U.S.A.* **107**, 21931–21936 (2010).
39. D. D. Bailey, Y. Zhang, B. J. van Soldt, M. Jiang, S. Suresh, H. Nakagawa, A. K. Rustgi, S. S. Aceves, W. V. Cardoso, J. Que, Use of hPSC-derived 3D organoids and mouse genetics to define the roles of yap in the development of the esophagus. *Development* **146**, dev178855 (2019).
40. Y. Zhang, Y. Yang, M. Jiang, S. X. Huang, W. Zhang, D. Al Alam, S. Danopoulos, M. Mori, Y. W. Chen, R. Balasubramanian, S. M. C. de Sousa Lopes, C. Serra, M. Bialecka, E. Kim, S. Lin, A. L. R. T. de Carvalho, P. N. Riccio, W. V. Cardoso, X. Zhang, H. W. Snoeck, J. Que, 3D modeling of esophageal development using human PSC-derived basal progenitors reveals a critical role for notch signaling. *Cell Stem Cell* **23**, 516–529.e5 (2018).
41. F. Murray-Zmijewski, D. P. Lane, J. C. Bourdon, p53/p63/p73 isoforms: An orchestra of isoforms to harmonise cell differentiation and response to stress. *Cell Death Differ.* **13**, 962–972 (2006).
42. A. B. Truong, M. Kretz, T. W. Ridky, R. Kimmel, P. A. Khavari, p63 regulates proliferation and differentiation of developmentally mature keratinocytes. *Genes Dev.* **20**, 3185–3197 (2006).
43. E. N. Kouwenhoven, M. Oti, H. Niehues, S. J. van Heeringen, J. Schalkwijk, H. G. Stunnenberg, H. van Bokhoven, H. Zhou, Transcription factor p63 bookmarks and regulates dynamic enhancers during epidermal differentiation. *EMBO Rep.* **16**, 863–878 (2015).
44. D. Aberdam, K. Gambaro, P. Rostagno, E. Aberdam, S. de la Forest Divonne, M. Rouleau, Key role of p63 in BMP-4-induced epidermal commitment of embryonic stem cells. *Cell Cycle* **6**, 291–294 (2007).
45. J. M. Pattison, S. P. Melo, S. N. Piekos, J. L. Torkelson, E. Bashkirova, M. R. Mumbach, C. Rajasingh, H. H. Zhen, L. Li, E. Liaw, D. Alber, A. J. Rubin, G. Shankar, X. Bao, H. Y. Chang, P. A. Khavari, A. E. Oro, Retinoic acid and BMP4 cooperate with p63 to alter chromatin dynamics during surface epithelial commitment. *Nat. Genet.* **50**, 1658–1665 (2018).
46. H. Watanabe, Q. Ma, S. Peng, G. Adelmant, D. Swain, W. Song, C. Fox, J. M. Francis, C. S. Pedamallu, D. S. DeLuca, A. N. Brooks, S. Wang, J. Que, A. K. Rustgi, K. K. Wong, K. L. Ligon, X. S. Liu, J. A. Marto, M. Meyerson, A. J. Bass, SOX2 and p63 colocalize at genetic loci in squamous cell carcinomas. *J. Clin. Invest.* **124**, 1636–1645 (2014).
47. D. K. Lee, Y. Liu, L. Liao, W. Li, D. Danielpour, J. Xu, Neuroendocrine prostate carcinoma cells originate from the p63-expressing basal cells but not the pre-existing adenocarcinoma cells in mice. *Cell Res.* **29**, 420–422 (2019).
48. C. M. Rudin, E. Brambilla, C. Faivre-Finn, J. Sage, Small-cell lung cancer. *Nat. Rev. Dis. Primers.* **7**, 3 (2021).
49. A. S. Ireland, A. M. Micinski, D. W. Kastner, B. Guo, S. J. Wait, K. B. Spainhower, C. C. Conley, O. S. Chen, M. R. Guthrie, D. Soltero, Y. Qiao, X. Huang, S. Tarapcsak, S. Devarakonda, M. D. Chalishazar, J. Gertz, J. C. Moser, G. Marth, S. Puri, B. L. Witt, B. T. Spike, T. G. Oliver, MYC drives temporal evolution of small cell lung cancer subtypes by reprogramming neuroendocrine fate. *Cancer Cell* **38**, 60–78.e12 (2020).
50. B. Vos, T. Rozema, R. C. Miller, A. Hendlisz, J. L. Van Laethem, K. Khanfir, D. C. Weber, I. El Nakadi, P. Van Houtte, Small cell carcinoma of the esophagus: A multicentre rare cancer network study. *Dis. Esophagus* **24**, 258–264 (2011).
51. E. Kim, M. Jiang, H. Huang, Y. Zhang, N. Tjota, X. Gao, J. Robert, N. Gilmore, L. Gan, J. Que, Isl1 regulation of Nkx2.1 in the early foregut epithelium is required for trachea-esophageal separation and lung lobation. *Dev. Cell* **51**, 675–683.e4 (2019).
52. F. Wang, D. B. Liu, Q. Zhao, G. Chen, X. M. Liu, Y. N. Wang, H. Su, Y. R. Qin, Y. F. He, Q. F. Zou, Y. H. Liu, Y. E. Lin, Z. X. Liu, J. X. Bei, R. H. Xu, The genomic landscape of small cell carcinoma of the esophagus. *Cell Res.* **28**, 771–774 (2018).
53. D. K. Lee, Y. Liu, L. Liao, F. Wang, J. Xu, The prostate basal cell (BC) heterogeneity and the p63-positive BC differentiation spectrum in mice. *Int. J. Biol. Sci.* **10**, 1007–1017 (2014).
54. T. Okumura, Y. Shimada, T. Omura, K. Hirano, T. Nagata, K. Tsukada, MicroRNA profiles to predict postoperative prognosis in patients with small cell carcinoma of the esophagus. *Anticancer Res* **35**, 719–727 (2015).
55. J. Moffat, D. A. Grueneberg, X. Yang, S. Y. Kim, A. M. Kloepfer, G. Hinkle, B. Piqani, T. M. Eisenhaure, B. Luo, J. K. Grenier, A. E. Carpenter, S. Y. Foo, S. A. Stewart, B. R. Stockwell, N. Hacohen, W. C. Hahn, E. S. Lander, D. M. Sabatini, D. E. Root, A lentiviral rnai library for human and mouse genes applied to an arrayed viral high-content screen. *Cell* **124**, 1283–1298 (2006).
56. A. Subramanian, P. Tamayo, V. K. Mootha, S. Mukherjee, B. L. Ebert, M. A. Gillette, A. Paulovich, S. L. Pomeroy, T. R. Golub, E. S. Lander, J. P. Mesirov, Gene set enrichment analysis: A knowledge-based approach for interpreting genome-wide expression profiles. *Proc. Natl. Acad. Sci. U.S.A.* **102**, 15545–15550 (2005).
57. H. S. Kaya-Okur, S. J. Wu, C. A. Codomo, E. S. Pledger, T. D. Bryson, J. G. Henikoff, K. Ahmad, S. Henikoff, CUT&Tag for efficient epigenomic profiling of small samples and single cells. *Nat. Commun.* **10**, 1930 (2019).

**Acknowledgments:** We thank all the lab members in Que's and Lu's labs for the discussion of the research and proofreading of the manuscripts. We thank C. Birchmeier-Kohler at the Max Delbrück Center for Molecular Medicine in Germany for providing the anti-INSM1 antibody. **Funding:** This work in the Que lab is supported by the National Institutes of Health (NIH) grants R01DK120650 and R01DK132251 (J.Q.), R01DE031873 and R01DK132251 (C.L.), P30DK132710 and R01CA272901 (T.C.W.), P01CA268991 (W.E.-R.), and P01CA098101 and P30CA013696 (A.K.R.) and by the National Natural Science Foundation of China grant nos. 32170831 (Y.Z.) and 81870380 (J.S.). D.K. acknowledges support from the NYSTEM training grant. Research reported in this publication was performed in the CCTI Flow Cytometry Core, supported, in part, by the Office of the Director, NIH, under award S10OD020056. The Columbia Center for Human Development Microscopy Core was supported by the NIH, Office of Research Infrastructure Programs, under grant S10OD032447. The Genetically Modified Mouse Models Shared Resource (GMMMSR) is supported by P30CA013696. **Author contributions:** Y.Z., D.K., H.L., C.L., and J.Q. conceived the study, designed the experiments, performed the experiments, analyzed the data, and drafted the manuscript. M.L., Y.F., M.J., X.C., S.S., H.H., J.S., F.S., J.L., D.L., J.C.A., and G.L. assisted in data collection and study design. P.Y., W.E.-R., A.Z., A.E.O., K.L., A.K.R., and T.C.W. critically revised the manuscript for important intellectual content. All authors read and approved the final manuscript. **Competing interests:** The authors declare that they have no competing interests. **Data and materials availability:** All data needed to evaluate the conclusions in the paper are present in the paper and/or the Supplementary Materials. Single-cell RNA sequencing (RNA-seq) data are available in the Gene Expression Omnibus (GEO) under accession number GSE263694. Bulk RNA-seq and CUT&Tag sequencing data are available in GEO under accession number GSE242464.

Submitted 24 April 2024
Accepted 4 September 2024
Published 9 October 2024
10.1126/sciadv.adq0479